JGR Atmospheres

RESEARCH ARTICLE
10.1029/2024JD042392

Contrasting Responses of Ion Concentration Variations to Atmospheric Patterns in Central Himalayan Ice Cores

Akane Tsushima[1,2], Nao Esashi[3], Sumito Matoba[4], Yoshinori Iizuka[4], Ryu Uemura[3], Kouji Adachi[5], Takeshi Kinase[5,6], Motohiro Hirabayashi[7], Kaoru Kawakami[4], Rijan B. Kayastha[8], and Koji Fujita[3]

[1]Graduate School of Science, Chiba University, Chiba, Japan, [2]Now at Graduate School of Integrated Science and Technology, Nagasaki University, Nagasaki, Japan, [3]Graduate School of Environmental Studies, Nagoya University, Nagoya, Japan, [4]Institute of Low Temperature Science, Hokkaido University, Sapporo, Japan, [5]Meteorological Research Institute, Tsukuba, Japan, [6]Japan Agency for Marine-Earth Science and Technology (JAMSTEC), Yokohama, Japan, [7]National Institute of Polar Research, Tokyo, Japan, [8]Himalayan Cryosphere, Climate and Disaster Research Center, Department of Environmental Science and Engineering, School of Science, Kathmandu University, Dhulikhel, Nepal

Abstract We analyzed the water-soluble chemical composition of an 81.2-m-long ice core collected in 2019 from ~6,000 m elevation on a south-facing glacier in the Nepal Himalaya. The ice core chronology is based on variability in nitrate and calcium ions, which reveal an apparently seasonal periodicity (with winter maxima) throughout the core's length. Two annual boundaries are consistent with the tritium peak representing nuclear tests conducted in 1963 CE and with the spike in sulfate ions due to the eruption of Krakatau in 1883 CE. The ice core spans 145 years from 1875 to 2019 CE. Dating uncertainties due to the layer counting methodology were estimated as ±1 year for 1963–2019 CE and ±2 years for 1875–1963 CE. Comparison with earlier ice cores drilled on the northern side of the Himalayas revealed that the ion components exhibit inverse correlations with two key climatic indices: the North Atlantic Oscillation and Southern Oscillation Index. Composite analysis of reanalysis climate data suggests that these inverse relationships reflect springtime pressure patterns, which show regional differences between the northern and southern sides of the Himalayan range.

Plain Language Summary The Himalayas present a major barrier to atmospheric flow, making ice cores, which preserve natural and anthropogenic aerosols, a valuable proxy for assessing both the climatic impact of the Himalayas and the dynamics of past climate variability. To date, however, relatively few ice cores have been collected from the Himalayas owing to logistical challenges. We obtained an 81.2-m-long ice core from a remote glacier on the southern side of the Himalayas and analyzed the water-soluble ions contained therein. Based on the seasonal variability in ion concentrations, we established that the ice core spans the period 1875–2019 CE. Comparison with neighboring ice cores from the northern side of the Himalayas revealed a heterogeneous relationship with climate indices. Specifically, our analysis of climate reanalysis data suggests that the contrasting surface pressure patterns occurring over the Tibetan Plateau in springtime impact the transport of aerosols to the ice core sites differently in the northern and southern sides of the Himalayas.

Key Points:

- Major ion concentrations were analyzed in an 81.2-m-long Himalayan ice core
- The ice core chronology was determined from cyclicity in nitrate and calcium ions and confirmed with atomic bomb and volcanic signals
- Contrasting relation between ions and climatic indices in neighboring ice cores reflects pressure field in spring over the Tibetan Plateau

Supporting Information:

Supporting Information may be found in the online version of this article.

Correspondence to:

K. Fujita,
cozy@nagoya-u.jp

Citation:

Tsushima, A., Esashi, N., Matoba, S., Iizuka, Y., Uemura, R., Adachi, K., et al. (2025). Contrasting responses of ion concentration variations to atmospheric patterns in central Himalayan ice cores. *Journal of Geophysical Research: Atmospheres*, *130*, e2024JD042392. https://doi.org/10.1029/2024JD042392

Received 5 SEP 2024
Accepted 8 JAN 2025

Author Contributions:

Conceptualization: Akane Tsushima, Koji Fujita
Data curation: Akane Tsushima, Sumito Matoba, Yoshinori Iizuka, Ryu Uemura, Kouji Adachi, Takeshi Kinase, Motohiro Hirabayashi, Kaoru Kawakami
Formal analysis: Akane Tsushima, Koji Fujita
Funding acquisition: Koji Fujita
Investigation: Akane Tsushima, Nao Esashi, Rijan B. Kayastha, Koji Fujita
Methodology: Akane Tsushima, Koji Fujita
Project administration: Rijan B. Kayastha, Koji Fujita

1. Introduction

Ice cores recovered from high elevation Himalayan glaciers provide valuable information on environmental change, human activity, and processes of atmospheric transport, the latter of which is influenced by variations in the summer monsoon and winter westerlies. To date, the Himalayan ice core inventory includes the Dasuopu (DP) cores, collected in 1997 from 7,200 m elevation on Mt. Shishapangma (Thompson et al., 2000), and the East Rongbuk (ER) cores, which were drilled in 1998 and 2002 from 6,500 m on Mt. Everest (Hou et al., 2003; Kang et al., 2002a; Kaspari et al., 2007; Qin et al., 2002) (Figure 1). Qin et al. (2002) reported different temporal trends in nitrate ($[NO_3^-]$) and sulfate ($[SO_4^{2-}]$) concentrations in the DP and ER cores: after the 1980s, nitrate and sulfate both decreased in the ER cores but increased in the DP cores despite the two sites being only 125 km apart. The two sites also exhibit contrasting accumulation records, although the ER record is generally consistent with data from three Tibetan ice cores (Kaspari et al., 2008; Pang et al., 2014; Yao et al., 2008). Although previous studies have suggested that this disparity reflects chronological errors in the DP cores (Hou et al., 2018, 2019) that argument remains speculative due to a dearth of comparative data. Indeed, the relative scarcity of accessible

Visualization: Koji Fujita
Writing – original draft: Akane Tsushima, Koji Fujita
Writing – review & editing: Nao Esashi, Sumito Matoba, Yoshinori Iizuka, Ryu Uemura, Kouji Adachi, Kaoru Kawakami

coring sites in the Himalayas (Takeuchi et al., 2020) underscores the critical need for additional ice core records from adjacent sites.

The climate of the central Himalayas is dominated by the Indian summer monsoon, which transports large amounts of moisture from the Indian Ocean; incursions of westerly airflow are common during the winter. Prior interpretations of Himalayan ice cores have suggested that mineral dust and anthropogenic pollutants are transported by these winter westerlies, whereas marine-derived ions are transported by the summer monsoon (Kang et al., 2002a; Kaspari et al., 2007; Thompson et al., 2000; N. Wang et al., 2002). Previous studies have also reported on the relationships between climatic indices and Asian ice core composition. For example, dust deposited in the Tien Shan and central Tibet is correlated with the North Atlantic Oscillation (NAO) (Y. Zhang et al., 2015; W. Zhang et al., 2017), whereas the accumulation rate and stable isotope composition of snowfall in northern Tibet are correlated with the NAO (Davis et al., 2005; N. Wang et al., 2003) and the El Niño-Southern Oscillation (ENSO/SOI) (N. Wang et al., 2003; X. Yang et al., 2014). Similarly, stable oxygen isotopes in central Tibetan precipitation have been correlated with ENSO and the Indian Ocean dipole mode index (DMI) (Joswiak et al., 2013) and with the Pacific Decadal Oscillation (Grigholm et al., 2009).

Apart from the correlations between the DP record and the NAO (Davis et al., 2005), the existing Himalayan ice core record is dominated by data from the ER cores, which show a negative relationship between dust content and the NAO (J. Xu et al., 2007) and inverse correlations between terrestrial- and ocean-sourced ions and the SOI (H. Xu et al., 2016). More broadly, investigations of multiple cores collected from the Tibetan Plateau also reported contrasting relationships between ice core components and climatic indices (Davis et al., 2005; Yao et al., 2008; D. Yang et al., 2022), including a few studies comparing the DP and ER cores both from the Himalayas (Kaspari et al., 2008; Qin et al., 2002). To date, however, there has been no comparative analysis of data from the northern and southern sides of the Himalayas given the lack of ice cores from the latter.

In this study, we measured the concentrations of soluble ions in an ice core drilled on the southern side of the Nepal Himalayas, and we used the wintertime maxima of nitrate and calcium to establish the depositional chronology. By comparing the interannual variability of major soluble ions with the variability in a core extracted from the northern side of the Himalayas, we explored the reportedly contrasting climatic responses of the two regions relative to climate reanalysis data.

2. Site and Methods

2.1. Ice Core Site and Preprocessing

In November 2019, we recovered an 81.2-m-long ice core (TB core) at 5,862 m elevation on the Trambau Glacier in the Rolwaling region of Nepal (Tsushima et al., 2021) (Figure 1). Mass balance observations suggest annual accumulation at this elevation is 730 ± 390 mm water equivalent (w.e.) (Sunako et al., 2019), and ice thickness at the drilling site is estimated to be ∼300 m (Farinotti et al., 2019). Due to budgetary and logistic constraints, we cut the ice core lengthwise and transported 60% of the entire core to Japan in a frozen state (Tsushima et al., 2021).

Ice core samples were prepared for measurement of major ion and tritium concentrations in the cold laboratory (−20°C) at the Institute of Low Temperature Science, Hokkaido University, Japan. First, we used a band saw to cut the core into 0.05 m sections. To minimize the risk of contamination (e.g., from drilling and transportation), we used a ceramic knife in a positive pressure environment to shave off the outer surface of each sample. Decontaminated samples (n = 1,592) were then packed in clean, sealed polyethylene bags and melted at ambient temperature after which the resulting water was transferred to polypropylene bottles for storage.

2.2. Analysis of Major Ions

Concentrations of major water-soluble ions ($[SO_4^{2-}]$, $[NO_3^-]$, $[Cl^-]$, $[NH_4^+]$, $[K^+]$, $[Mg^{2+}]$, $[Ca^{2+}]$, and $[Na^+]$ in ppb) were quantified using Dionex ICS-1100 and ICS-2100 ion chromatography systems (Thermo Scientific). The measurement precision for each ionic species was 10%; we corrected for measurement bias by multiple measurements of the same sample. For SO_4^{2-} and Ca^{2+}, we calculated their non-sea salt (*nss*) fractions as follows:

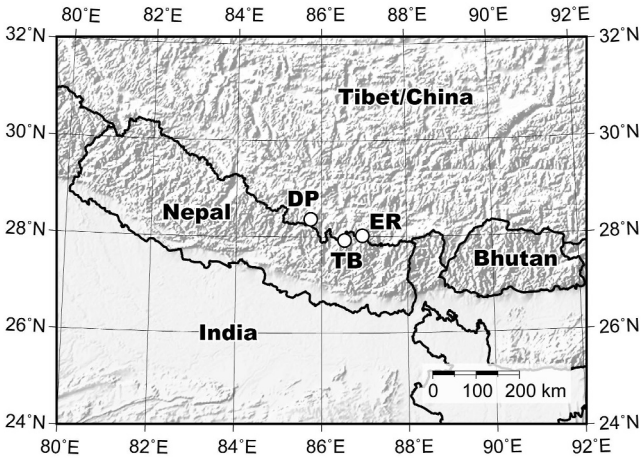

Figure 1. Locations of the ice core sites. TB, DP, and ER denote Trambau (this study), Dasuopu (Thompson et al., 2000), and East Rongbuk (Qin et al., 2002) ice core sites, respectively.

$$\begin{aligned}\left[nssSO_4^{2-}\right] &= \left[SO_4^{2-}\right] - \left(SO_4^{2-}/Na^+\right)_{sea} \times \left[Na^+\right],\\ \left[nssCa^{2+}\right] &= \left[Ca^{2+}\right] - \left(Ca^{2+}/Na^+\right)_{sea} \times \left[Na^+\right],\end{aligned} \quad (1)$$

where $\left(SO_4^{2-}/Na^+\right)_{sea}$ and $\left(Ca^{2+}/Na^+\right)_{sea}$ are the mass ratios of SO_4^{2-} (0.252) or Ca^{2+} (0.0432) to Na^+ in seawater, respectively (Keene et al., 1986; Legrand & Mayewski, 1997). Tritium concentrations were analyzed by liquid scintillation counting (LSC-LB3; Aloka, Japan) at the National Institute of Polar Research. First, we measured all layers at a coarse resolution (2.5 m intervals, $n = 32$ samples) by mixing each 1 mL from every 50 samples. To confirm the data at depths at which high tritium concentrations were measured, we made a second measurement for ice layers at depths between 29.77 and 35.11 m (0.25 m intervals, $n = 20$ samples) by mixing each 10 mL from every 5 samples.

2.3. Dating Procedure

Previous investigations of the chemical composition of Himalayan aerosols, snow pack, and glacier ice have reported high concentrations and an apparent seasonality (high in winter and low in summer) for the ions $\left[SO_4^{2-}\right]$, $\left[NO_3^-\right]$, $\left[Ca^{2+}\right]$, and $\left[NH_4^+\right]$ (Kumar & Raman, 2016; Tripathee et al., 2017). Elevated $\left[Ca^{2+}\right]$ are linked to dust originating in the arid regions of southwestern Asia, the Middle East, and Africa during the non-monsoon season (J. Xu et al., 2010). The seasonality of this flux has been confirmed in the Everest region by comparison with oxygen isotope ratio maxima, which represent the winter monsoon phase (Kang et al., 2004). In the northwestern Himalayas, for instance, Tian and Tian (2019) employed the seasonal distributions of $\left[NO_3^-\right]$ and $\left[NH_4^+\right]$ as biogenic ions and of $\left[Ca^{2+}\right]$ and $\left[Mg^{2+}\right]$ as dust origin indicators to establish an age scale for the Qiangyong ice core.

To construct an age scale for the TB ice core, we took the $\left[NO_3^-\right]$ and $\left[Ca^{2+}\right]$ peaks to represent annual winter boundaries. Of all the major ions measured, $\left[NO_3^-\right]$ and $\left[Ca^{2+}\right]$ exhibit the highest concentrations and clearest cyclicity. We removed noise and extracted the winter peaks following a specific protocol. First, assuming a mean annual accumulation rate of 0.7 m w.e. (Sunako et al., 2019), we calculated anomalies from the 13-point (0.65 m w.e.) running mean for both $\left[NO_3^-\right]$ and $\left[Ca^{2+}\right]$. We then screened positive anomalies, selecting the largest peak within a 3-point data range (i.e., the bounding points above the anomaly) as the likely winter peak for that year. We made this selection for all layers by shifting points sequentially from the surface to the bottom of the core. Third, we calculated the median value of all selected peaks ($\left[NO_3^-\right]$ or $\left[Ca^{2+}\right]$, or both) and rejected any that fell below the values. Finally, when multiple peaks occurred within four adjacent points, we rejected the lower peaks on the basis that neighboring maxima are unlikely to exhibit multiple boundaries within a single year. The resulting chronology was validated against the 1963 tritium peak and a number of $\left[SO_4^{2-}\right]$ peaks associated with volcanic events.

2.4. Climatic Indices and Inter-Core Comparison

We compared the major ions in the TB core with climatic indices, including the NAO (Barnston & Livezey, 1987; Chen & van den Dool, 2003; van den Dool et al., 2000), SOI (Allan et al., 1991; Können et al., 1998), DMI (Saji & Yamagata, 2003), and Atlantic Multidecadal Oscillation (AMO) (Enfield et al., 2001; Chylek et al., 2012; C. Wang et al., 2012), which have identified as significant components of ice core chemistry. NAO represents the atmospheric pressure pattern between the Icelandic Low and the Azores High, which affects atmospheric circulations around high mountain Asia through altering westerly jets (Gong et al., 2011). SOI is computed from surface air pressure anomalies at Darwin, Australia, to pressure anomalies at Tahiti indicating indicate the strength of the Walker Circulation whereas DMI represents the west-southeastern gradient of sea surface temperature (SST) over the equatorial Indian Ocean, both affect the Indian summer monsoon through ENSO and Indian Ocean dipole (e.g., Ashok et al., 2001; Webster & Yang, 1992). AMO represents the SST anomalies over North Atlantic Ocean with an estimated period of 60–80 years (Enfield et al., 2001). We also compared the TB core chemistry with those of the ER (Hou et al., 2003) and DP (Thompson et al., 2000) cores though the available

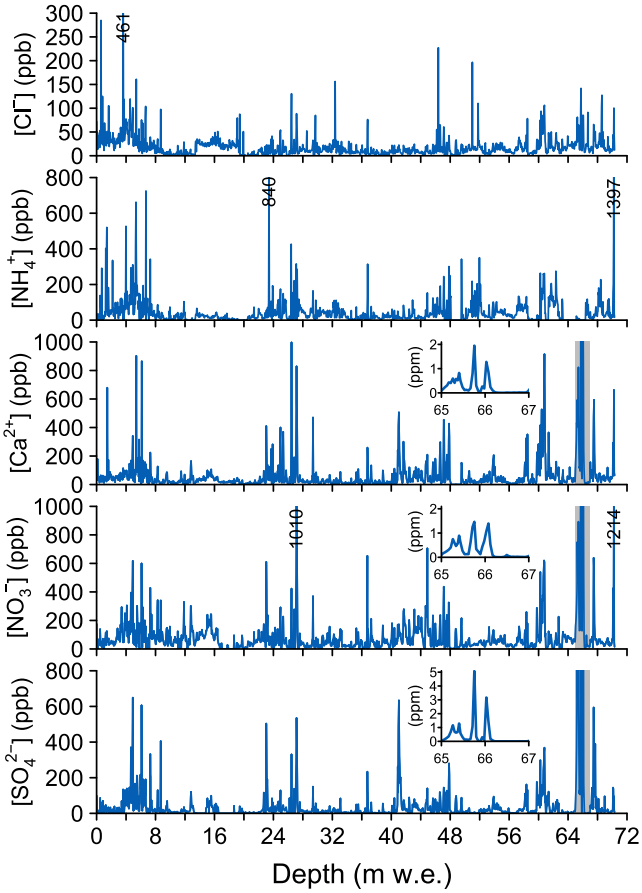

Figure 2. Ion concentrations along ice core depth of the TB core. Inset figure of $[Ca^{2+}]$, $[NO_3^-]$, and $[SO_4^{2-}]$ is the close up of the gray shading part between 65 and 67 m w.e. Values shown in $[Cl^-]$, $[NH_4^+]$, and $[NO_3^-]$ denote overshoot spikes in ppb. $[Na^+]$ is not shown because of the similar fluctuation with $[Cl^-]$. $[K^+]$ and $[Mg^{2+}]$ are not shown because of their low concentrations (<120 ppb).

ion data for the DP core are limited to $[Cl^-]$, $[NO_3^-]$, and $[SO_4^{2-}]$. Upon observing significant correlations between the ice core ion and NAO or SOI, we made composite analyses on both the high and low indices using ERA5 reanalysis data (Hersbach et al., 2020).

3. Results

3.1. Overview of Ion Concentrations

We used the density profile (Tsushima et al., 2021) to convert the 81.2 m TB ice core depth to a 70.31 m w.e. depth. Figure 2 depicts the variability in concentrations of major ions in the core. Both $[NO_3^-]$ and $[Ca^{2+}]$ maintain high concentrations (the averages for the entire ice core were 80.4 and 60.2 ppb, respectively) and exhibit synchronous periodic fluctuations. Relative to the core average of 41.4 ppb, $[SO_4^{2-}]$ exhibits remarkably large peaks (> 1 ppm) at 65.0–66.2 m w.e.; with the exception of this layer, concentrations of $[SO_4^{2-}]$ fluctuate synchronously with $[NO_3^-]$ and $[Na^+]$. $[NH_4^+]$ shows high (79.0 ppb) concentrations between the surface and 8 m w.e., with lower (19.7 ppb) concentrations between 8 and 24 m w.e.; the core average for $[NH_4^+]$ is 42.3 ppb.

The ion balance chart suggests that the TB core is characterized by high $[Ca^{2+}]$, $[NH_4^+]$, $[NO_3^-]$, and $[SO_4^{2-}]$, and relatively low $[Na^+]$, $[Cl^-]$, $[Mg^{2+}]$, and $[K^+]$ (Figure 3a). Figure S1 in Supporting Information S1 shows the relationships between $[Na^+]$ and $[Cl^-]$ and between the total and non-sea salt (*nss*) components of $[SO_4^{2-}]$ and $[Ca^{2+}]$, respectively. $[Na^+]$ and $[Cl^-]$ deviate significantly from the sea salt ratio (1.78; dashed line in Figure S1a in Supporting Information S1), suggesting that they do not maintain the compositional ratio of sea salt (Figure S1a in Supporting Information S1). Total $[SO_4^{2-}]$ and $[Ca^{2+}]$ reflect the *nss* components, indicating that concentrations of sea-salt composition are generally low in the TB core. $[Na^+]$ is one third hold to $[SO_4^{2-}]$ and one fourth hold to $[Ca^{2+}]$, respectively (Figures S1b and S1c in Supporting Information S1).

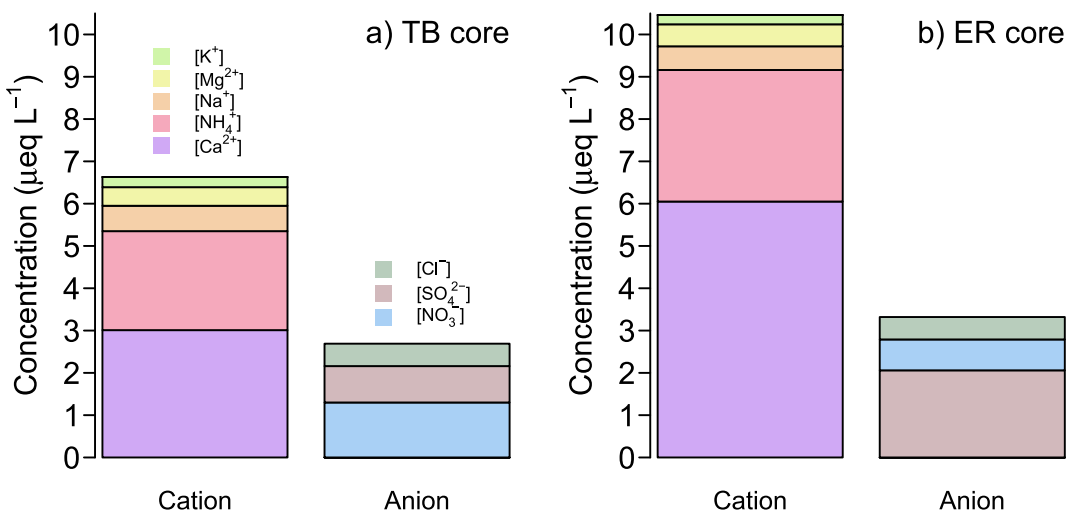

Figure 3. Ion balance of mean concentrations in the (a) TB and (b) ER cores.

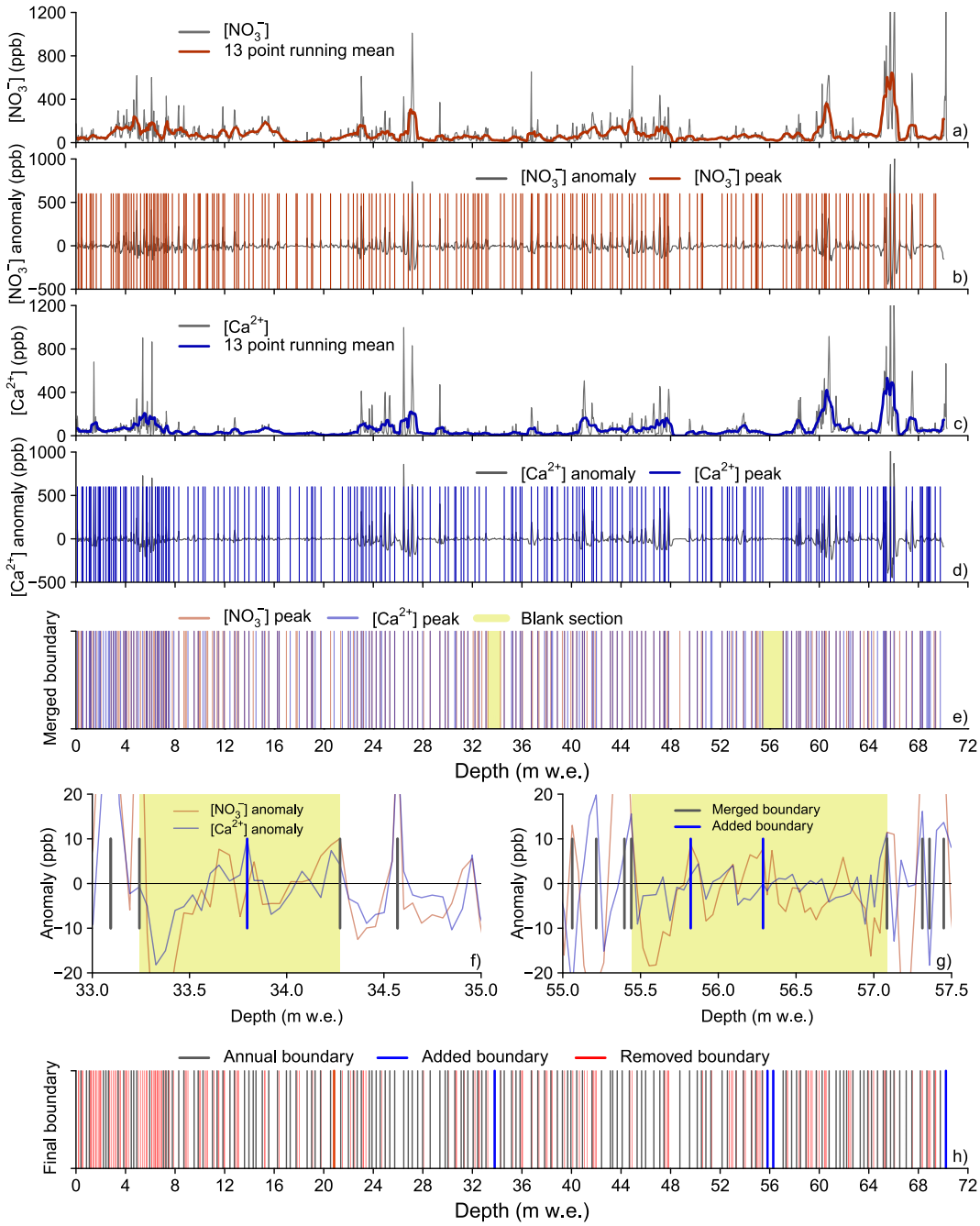

Figure 4. Dating procedure of the TB core. (a) A 13-year running mean was obtained for $[NO_3^-]$, (b) anomaly from the running mean was calculated, and then positive peaks were selected as candidate annual boundary. (c and d) the same procedure was applied to $[Ca^{2+}]$ and then (e) merged into one. (f and g) three annual boundaries were added at the two blank sections (blue lines in (h)). (h) by removing "too nearby" boundaries (red lines), annual boundary was determined (black lines). Thick red line at 20.84 m denotes the manually removed boundary based on the validation (Section 3.2).

3.2. Validation of Ice Core Chronology

The anomalies in the 13-point running mean are shown in Figures 4a and 4c, whereas annual boundary candidates (those peaks exceeding the median) are shown in Figures 4b and 4d. Merged $[NO_3^-]$ and $[Ca^{2+}]$ candidate peaks are displayed in Figure 4e. We identified two sections (33.24–34.27 and 55.44–57.08 m w.e.) for which no peak was detectable (yellow shading in Figure 4e). $[NO_3^-]$ and $[Ca^{2+}]$ are relatively low (30.9 and 12.5 ppb, respectively) in

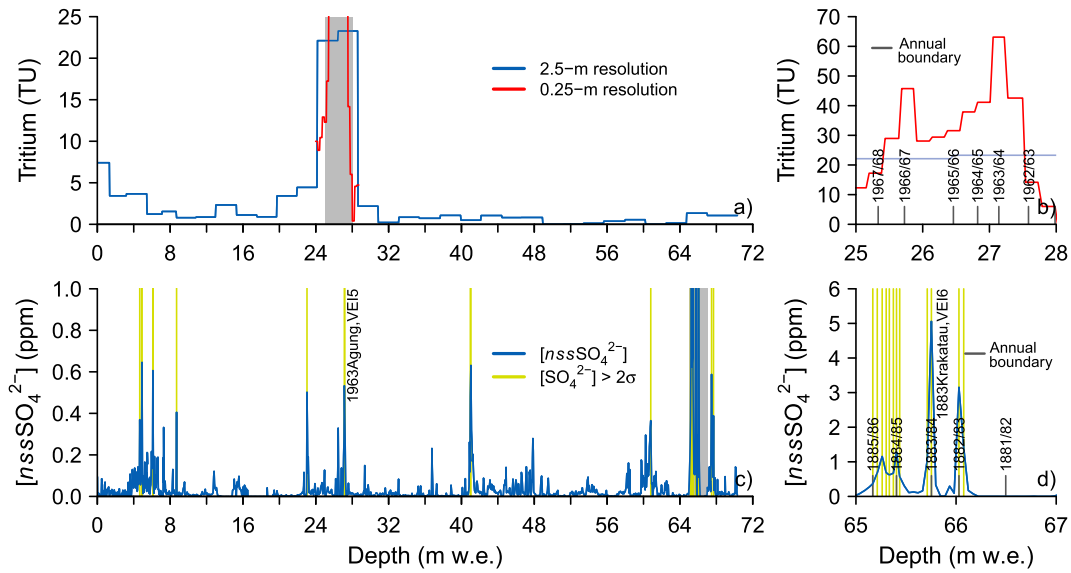

Figure 5. Validation of the chronology for the TB core. Year at each annual boundary denote the end of each year. One year difference at the 1963 tritium peak and the 1883 Krakatau $[nssSO_4^{2-}]$ peak are corrected by removing one annual boundary at 20.84 m w.e. depth (thick red line in Figure 4h). See details in Section 3.2.

both, prompting us to add three peaks manually (Figures 4f and 4g). After adding one further annual boundary near the base of the core (70.23 m w.e.), we removed any smaller neighboring peaks from layers in which multiple peaks were detected within four adjacent points. Figure 4h depicts the annual boundaries for the entire core, whereas $[NO_3^-]$ and $[Ca^{2+}]$ anomalies and any boundaries that were removed or added manually are shown in Figure S2 in Supporting Information S1.

Figure 5 contains the tritium and $[SO_4^{2-}]$ data we used to validate the ice core chronology. Specifically, Figure 5a shows tritium profiles at two different resolutions (2.5 and 0.25 m w.e.); the largest tritium peak, at 27.05–27.22 m w.e., corresponds to the 1962/63 boundary determined via annual layer counting (Figure 5b). This tritium peak is associated with nuclear tests in 1963 and is a common reference layer in Asian ice cores (e.g., Hou et al., 2018, 2019; Thompson et al., 2000).

Given the relative infrequency of large volcanic eruptions and the effective removal of atmospheric SO_4^{2-} within 1–2 years of an eruption, volcanic SO_4^{2-} signals appear as narrow spikes in ice cores (Moore et al., 2002). We flagged $[nssSO_4^{2-}]$ spikes greater than 2σ (Figure 5c) as representing large volcanic eruptions. Of particular note, we correlate the largest $[nssSO_4^{2-}]$ spike (5.06 ppm, 28.8σ), which occurs at 65.75 m w.e., adjacent to the 1882/83 boundary, with the 1883 eruption of Krakatau (volcanic eruption index (VEI) = 6 (Rampino & Self, 1982)). This association is supported by elevated $[nssSO_4^{2-}]$ at depths between 65.17 and 66.03 m w.e., corresponding to the period 1881–1884 (Figure 5d). Prior work has shown that high SO_4^{2-} persisted in the stratosphere for several years after the Krakatau eruption (Rampino & Self, 1982). Furthermore, assuming that the mean 1963–2019 accumulation rate (0.484 m w.e. a^{-1}) can be applied on longer timescales, the 1883/84 boundary is estimated to be 65.82 m w.e., which aligns well with both the 1883/84 boundary (65.71 m w.e.) and the maximum $[nssSO_4^{2-}]$ (65.75 m w.e.).

A prominent spike in $[nssSO_4^{2-}]$ (533 ppb, 3.0σ) at 27.14 m w.e. (Figure 5c) probably correlates with the large 1963 eruption of Mt. Agung in Indonesia (VEI = 4 (Delmas & Boutron, 1978; Hammer, 1980; Rampino & Self, 1982)). Upon removing a minor peak at 20.84 m w.e. (thick red line in Figure 4h), which is the smallest peak at depths < 24 m w.e., we take the tritium peak and the largest $[nssSO_4^{2-}]$ peak to represent the boundaries of 1963/64 and 1883/84, respectively (Figures 5b and 5d). On this basis, we estimated that the 70.31 m w.e. ice core spans the period between 1875 and 2019.

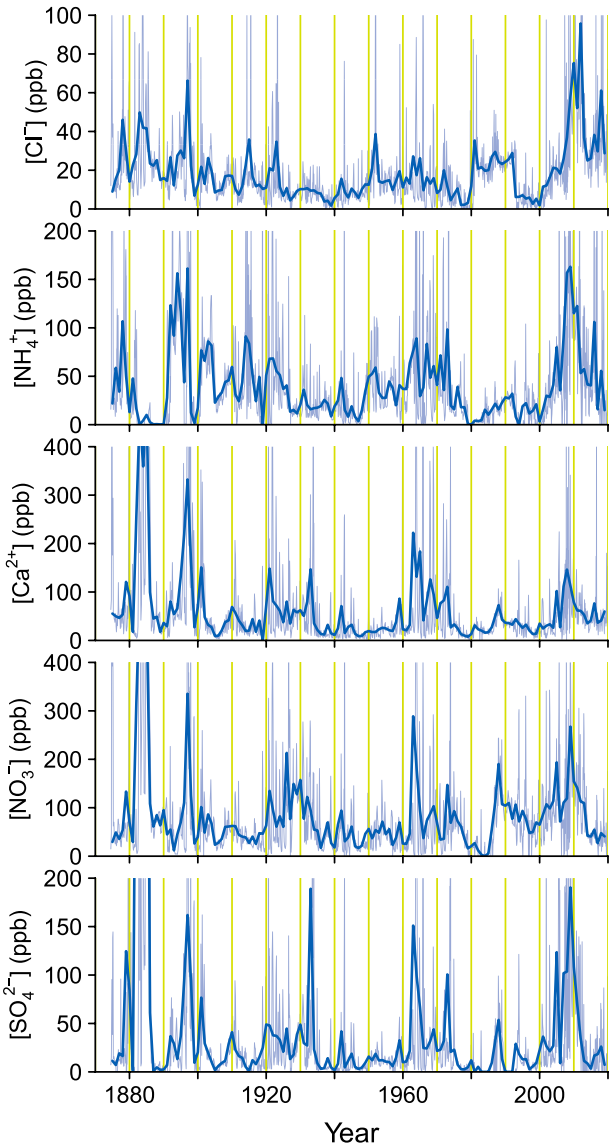

Figure 6. Annual mean major ions in the TB core. Thin blue and yellow lines denote the original values and decadal boundary, respectively. Close up figures for overshooting period (1880–1900) for $[Ca^{2+}]$, $[NO_3^-]$, and $[SO_4^{2-}]$ are shown in Figure S3 in Supporting Information S1.

3.3. Temporal Variability in Ion Concentrations

Annual variations in the concentrations of major ions are shown in Figure 6, and the correlation coefficients among the annual mean values are summarized in Figure 7a and Table S1 in Supporting Information S1. $[Na^+]$ and $[Cl^-]$ exhibit similar variability and thus return high correlation coefficients ($r = 0.84$); both ions maintain high levels in the 1880s, 1890s, and 2010s with an extended period (>10 years) of elevated concentration from 1980. The other measured ions ($[Ca^{2+}]$, $[NO_3^-]$, and $[SO_4^{2-}]$) show a similar variability ($r > 0.87$) with extremely high concentrations in the 1880s (Figure S3 in Supporting Information S1) and additional peaks in the 1890s, 1920s–1930s, 1960s–1970s, and around 2010 ($r > 0.59$). Although there is no evidence that Ca^{2+} and NO_3^- were produced by the Krakatau eruption, high concentrations of these ions have been reported in the ER core for the early 1880s (Qin et al., 2002). Both $[K^+]$ and $[Mg^{2+}]$ occur in low (<120 ppb) relative to other ions and thus are not shown in Figure 6. Nonetheless, $[K^+]$ and $[Mg^{2+}]$ are positively correlated with $[Ca^{2+}]$, $[NO_3^-]$, and $[SO_4^{2-}]$ ($r > 0.49$; Figure 7a). Although $[NH_4^+]$ is the sole ion behaving differently from the other measured ions in our record (Figure 7a; Table S1 in Supporting Information S1), a moderate correlation between $[NH_4^+]$ and $[Cl^-]$ ($r = 0.49$) might reflect a pseudo-relationship, since $[Na^+]$ and $[Cl^-]$ fluctuate in tandem ($r = 0.84$).

3.4. Comparisons With Other Himalayan Ice Cores and Climate Indices

We compared the major ions in the TB core with those reported from the ER core, which was recovered from the northern side of Mt. Everest (Kang et al., 2002a). Ion balance charts reveal generally lower concentrations in the TB core than in the ER core (63% for cations and 81% for anions; Figure 3) with this difference being dominated by $[Ca^{2+}]$, $[NO_3^-]$, and $[SO_4^{2-}]$. Concentrations of the remaining ions are similar between the two cores. We note that $[NO_3^-]$ is higher in the TB core (48% of all measured anions), whereas $[SO_4^{2-}]$ is the dominant ion in the ER core (62% of all measured anions). Correlation coefficients are similarly positive among ions in the ER core, though $[NH_4^+]$ and $[K^+]$ exhibit different tendency from those in the TB core (Figure 7). Kang et al. (2002b) and Hou et al. (2003) highlighted the unique behavior of $[NH_4^+]$ in the ER cores relative to the other ions, although correlations are more significant in the ER cores than in the TB core (Figure 7). In general, however, ion combinations in both cores are not significantly correlated between the two sites ($-0.21 < r < 0.08$). Three ions in the DP core ($[Cl^-]$, $[NO_3^-]$, and $[SO_4^{2-}]$) also show no significant correlations with the ion concentrations in the TB core ($-0.19 < r < 0.04$).

We compared major ions in the TB and ER data sets with the climate indices listed in Section 2.4 (Figure 8; Tables S3 and S4 in Supporting Information S1). Although mean annual values in the two cores exhibit low correlation coefficients with the indices ($|r| < 0.37$), the 5-year running mean values show generally significant correlations between multiple ions and the NAO_{5yr} (Figure 9). Furthermore, although $[NH_4^+]$ and $[SO_4^{2-}]$ both exhibit weak correlations with the DMI_{5yr} and AMO_{5yr}, the correlation matrix does not show a clear and consistent relationship. In the two cores, we note that $[NH_4^+]$ alone displays a significant correlation with the SOI_{5yr} (Figure 10). Results of the DP core show more significant correlations with NAO, SOI, and DMI, although only three ions are available (not shown in figure but listed in Table S5 in Supporting Information S1). Another notable feature of the correlation charts is the contrasting signs (positive or negative) of correlations between the two cores and some indices (Figure 8). For instance, ions in the TB core exhibit negative correlations with the NAO_{5yr}, whereas those in the ER core are positively correlated. Although the other indices do exhibit weak correlations

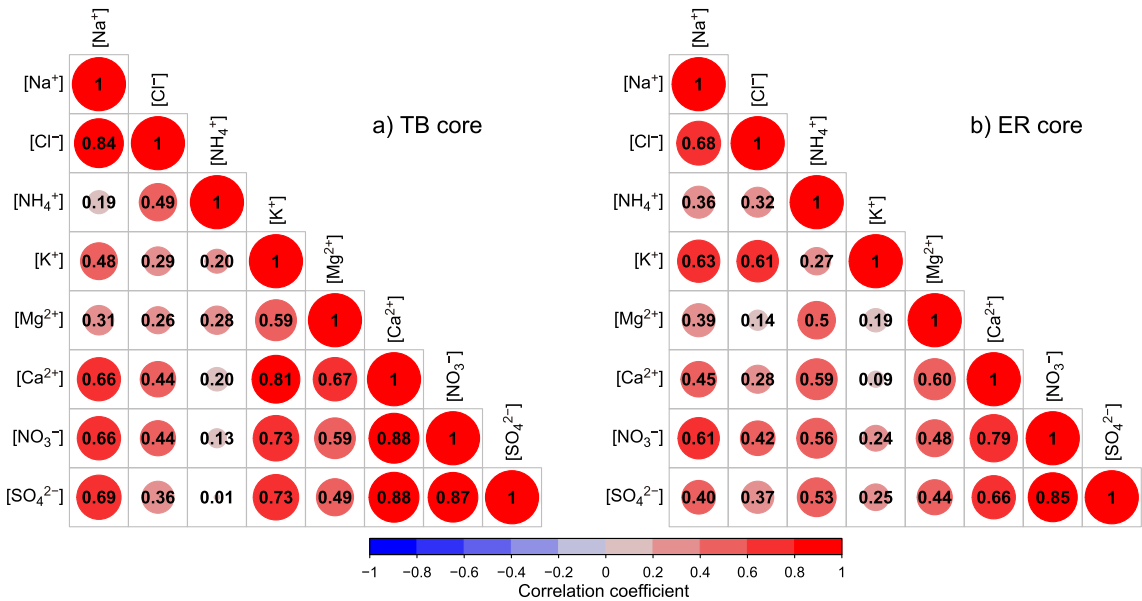

Figure 7. Correlation coefficients among the major ions in (a) TB and (b) ER cores. Correlation values are listed in Tables S1 and S2 in Supporting Information S1.

(with the exception of $[NH_4^+]$ and the SOI_{5yr}), there is generally a contrasting pattern between the TB and ER records despite the sites being located only 40 km apart. The signs of correlations for the DP core are similar to those for the ER core, which is also located in the northern side of the Himalayan range. We discuss possible causes for this disparity in Section 4.3.

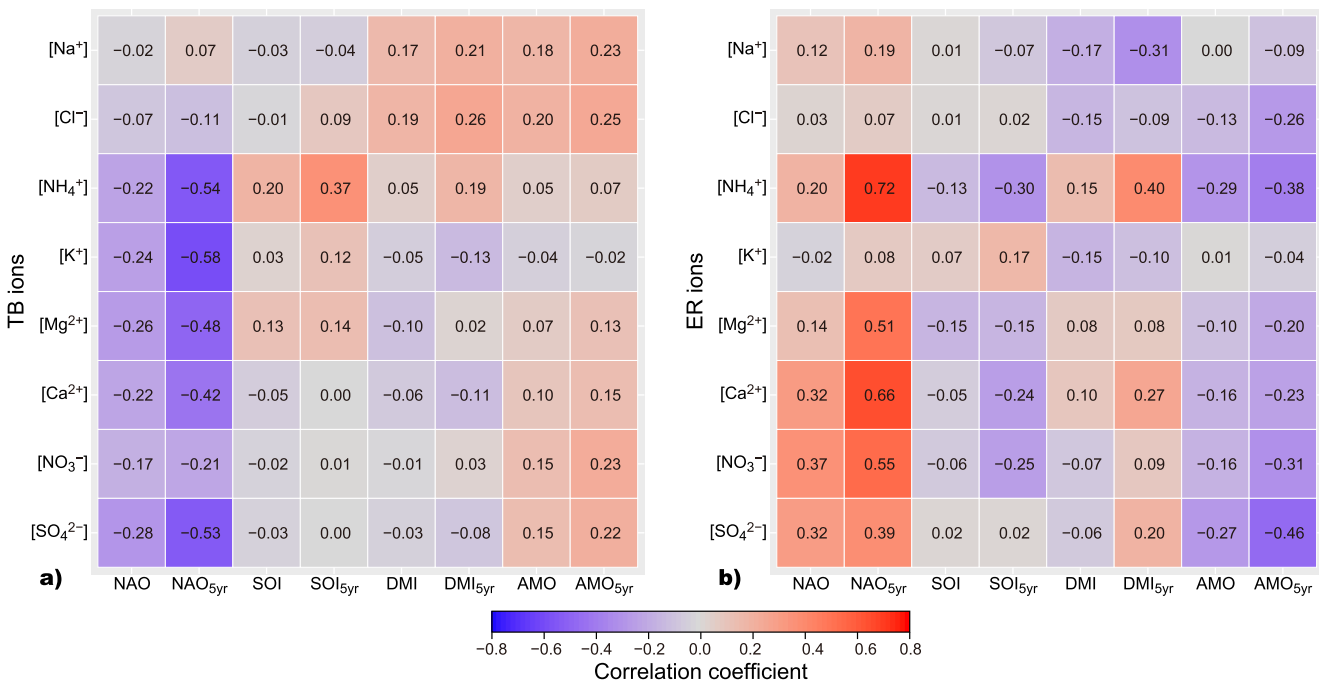

Figure 8. Correlation coefficients of the major ions in (a) TB and (b) ER cores against climate indices. Subscript 5yr denotes the correlations among the 5-year running means. Correlation values are listed in Tables S3 and S4 in Supporting Information S1.

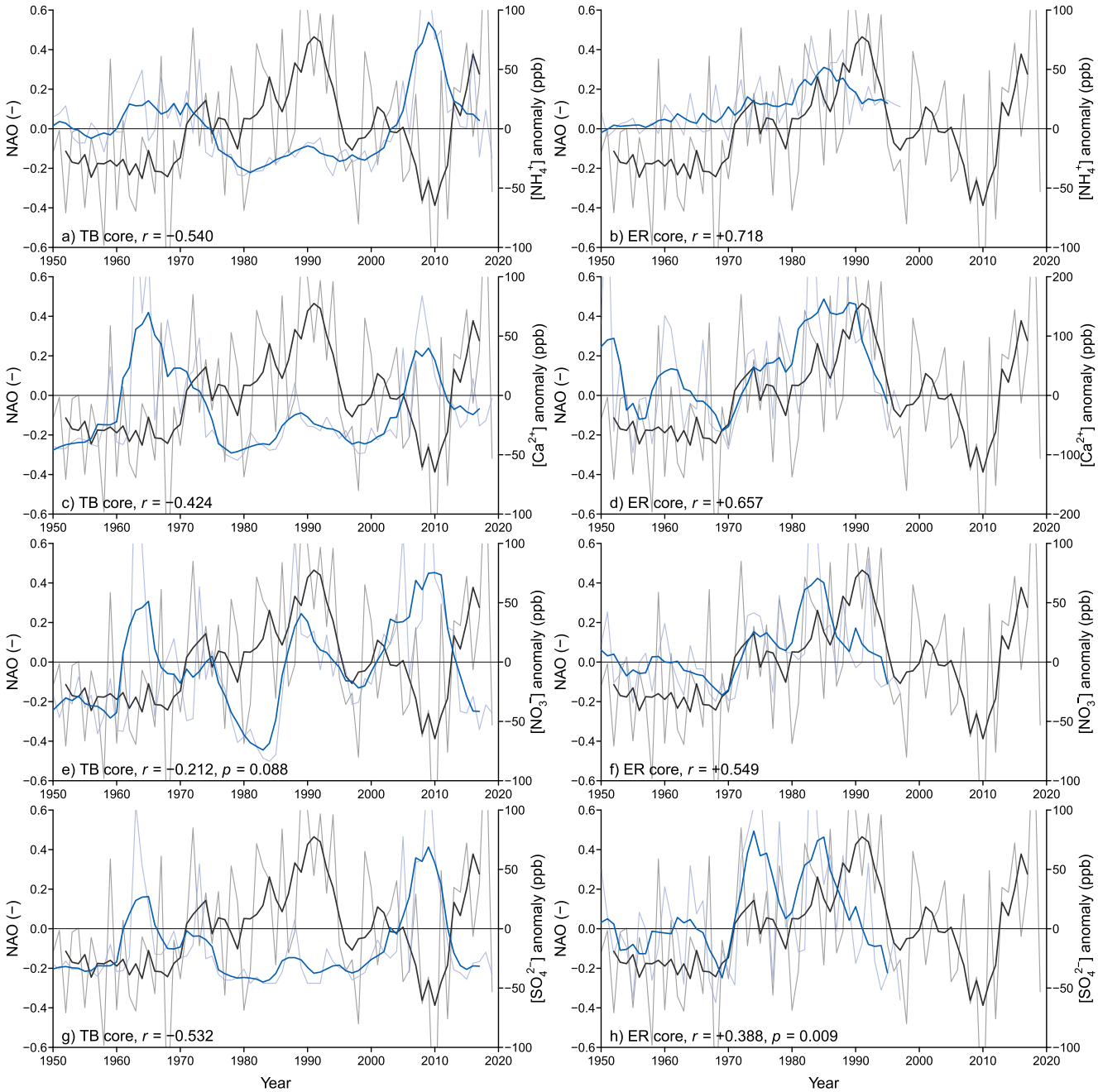

Figure 9. Annual (thin lines) and 5-year running mean (thick lines) of NAO (black, left axis) and ion anomalies (blue, right axis; in order of (a and b) $[NH_4^+]$, (c and d) $[Ca^{2+}]$, (e and f) $[NO_3^-]$, and (g and h) $[SO_4^{2-}]$ from up to bottom panels) in TB (left panels) and ER (right panels) cores. Note that the right scale of panel (d) is different from other panels. Significance level of the correlation coefficients without p-value is $p < 0.001$.

4. Discussion

4.1. Chronological Uncertainty

We evaluated the chronological uncertainty of our record by changing the number of points in the running mean used in the first step (initially 13−points). Throughout the ice core, the error in annually counted layers was −1 year using the 11-point running mean and +3 years using the 15-point running mean.

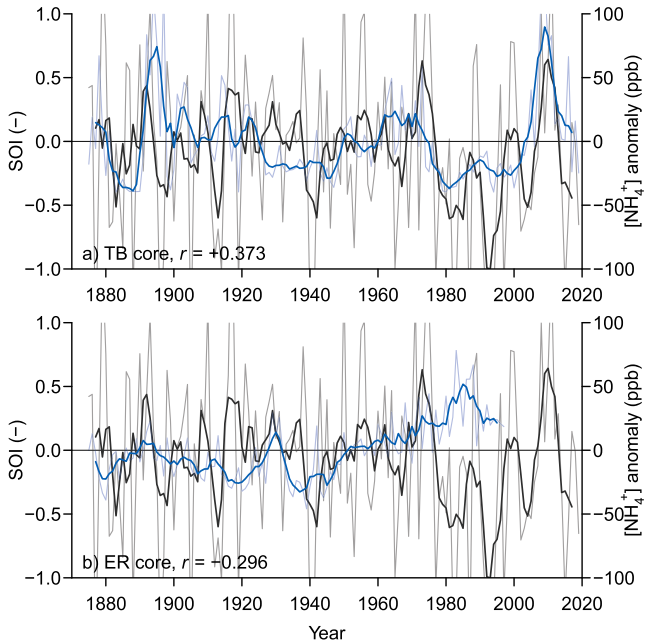

Figure 10. Annual (thin lines) and 5-year running mean (thick lines) of SOI (black, left axis) and $[NH_4^+]$ anomaly (blue, right axis) in (a) TB and (b) ER cores.

Despite being the largest volcanic sulfate spike observed in our TB core, we note that the Krakatau eruption was not detected in the DP core or in the Belukha ice core from the Russian Altai (Okamoto et al., 2011; Olivier et al., 2006; Thompson et al., 2000). At Belukha, a volcanic signal might be obscured by the high background sulfate levels due to dust deposition at that time (Aizen et al., 2016; Olivier et al., 2006). In the ER core, the Pinatubo (1991), Agung (1963), and Tambora (1815) eruptions have been identified using Bismuth as an indicator of volcanic input (Kaspari et al., 2007; J. Xu et al., 2009), whereas the Krakatau event is detectable solely on the basis of sulfate (Qin et al., 2002). For the TB core, we correlated the 1963 $[nssSO_4^{2-}]$ spike with the Agung eruption (Figure 5c) but could find no corresponding spike for the Pinatubo event (Figure 6).

An additional time marker is the failed monsoon of 1876–1877, which is manifested in the DP and ER cores as maxima in $[Cl^-]$ and dust (Kang et al., 2002a; Thompson et al., 2000). In the bottom part of the TB core, which dates to 1874, the concentration of $[Cl^-]$ (100 ppb) is much higher than that in the same layer in the DP core yet is not significantly different from the overall TB and ER time series. One explanation for this result is that the largest ion spikes assumed to date to 1883 actually correspond to the 1877 drought (Figure 6 and Figure S3 in Supporting Information S1), in which case the age uncertainty might be as much as 5 years for the bottom of the core (~1880s). We reject this scenario, however, because the $[Cl^-]$ peak for this period is not significant (~50 ppb).

The three Himalayan ice cores do not exhibit consistent patterns in accumulation (Kaspari et al., 2008; Pang et al., 2014), volcanic horizons (Kaspari et al., 2007; J. Xu et al., 2009), or drought events (Kang et al., 2002a; Thompson et al., 2000). Furthermore, major ion distributions in the two adjacent cores (TB and ER) cannot be correlated between sites as discussed below (Section 4.3). Taken together, this lack of regional consistency suggests that there is no single uniform horizon for validating ice core chronologies throughout the Himalayas. Together with the 1-year error reported above (Section 3.2), the TB ice core chronology potentially exhibits age uncertainties of ±1 year between 1963 and the present and of ±2 years between 1875 and 1963.

The TB density profile suggests that the core site has been affected by melting and refreezing (Tsushima et al., 2021). In particular, the blank sections could have been affected by meltwater, which would smooth signals of the ion concentrations in the snowpack. Although it has been found that Ca^{2+}, used in the dating procedure, formed more prominent peaks in snowpack in the Himalayas than other ions (Kumar & Raman, 2016; Tripathee et al., 2017), it is sensitive to meltwater (Brimblecombe et al., 1985; Virkkunen et al., 2007). Previous studies demonstrated that soluble ion species were eluted down by meltwater whereas stable isotope stratigraphy remained relatively unchanged in snow layers on a temperate glacier (Pang et al., 2007, 2012). We find that small signals were also observed in the water stable isotope ($\delta^{18}O$, not shown), which is not inconsistent with the annual layer identification by ions. We calculated the coefficient of variation (CV) and the ratio of maxima to minima (MXMN) for each annual layer of the TB and ER cores before calculating mean values for both (Table S6 in Supporting Information S1). The CV is defined as the standard deviation divided by the mean, whereas MXMN is calculated as the mean of three highest values divided by that of three lowest values (excluding zero values). The CV values for the TB core (3.6 – 58) are much larger than those of the ER core (0.6 – 1.1), whereas MXMN ratios in the TB core (4.3 – 9.2) are smaller than those in the ER core (4.5 – 25). We also note that the ion balance charts reveal similar concentrations of marine-derived ions ($[Na^+]$, $[K^+]$, $[Mg^{2+}]$, $[Cl^-]$) between the two cores (Figure 3). Thus, on the basis of these comparisons, we conclude that meltwater percolation has had no significant impact on the seasonal cyclicity of ions preserved in the TB core.

4.2. Temporal Variability in Anthropogenically Sourced Ions

The temporal variations in $[NO_3^-]$ and $[SO_4^{2-}]$ aerosols, both of which have anthropogenic sources, exhibit a high correlation in our record ($r = 0.87$). Following generally synchronous fluctuations throughout the 20th

Century, $[NO_3^-]$ began to rise in the mid-1980s, whereas concentrations of $[SO_4^{2-}]$ have increased since 2000. Ice core records from Greenland and the European Alps document a pronounced rise in sulfate emissions from North America and Europe since the onset of the Industrial Revolution (~1850s) with declining values after the 1970s linked to greater regulation of atmospheric pollutants (Iizuka et al., 2018). In contrast, sulfate levels in South Asia increased six-fold between 1951 and 1997 (Smith et al., 2001); $[SO_4^{2-}]$ concentrations in the DP core increased by a factor of 2.5 during the same period (Duan et al., 2007).

Figure S4 in Supporting Information S1 shows fluctuations in NO_x, SO_2, and NH_3 emissions from Europe, South Asia, and China, data for which were obtained from the Community Emissions Data System (Hoesly et al., 2018). Countries included in Europe and South Asia are listed in Table S7 in Supporting Information S1. Given the geographical context that the Himalayas is located upwind of the main emission sources in China, it might be pertinent to focus on the emissions from South Asia and Europe. Although fossil-fuel-derived NO_x and SO_2 emissions in Europe have been high level from the beginning of the 20th century and then decreased since the 1980s, those in South Asia have risen continuously since the late 1960s (Figures S4a and S4b in Supporting Information S1). With the exception of recent negative trends (in the 2010s), the variability in $[NO_3^-]$ and $[SO_4^{2-}]$ levels in the TB core is significantly different from measured anthropogenic emissions over the same period even including that from China. Neither $[NO_3^-]$ nor $[SO_4^{2-}]$ exhibit a significant increase despite rising NO_x and SO_2 emissions. Similarly, NH_3 emissions from the three regions show no correlative fluctuations with $[NH_4^+]$ in the TB core (Figure S4c in Supporting Information S1). We suggest, therefore, that decadal-scale fluctuations in ice core $[NO_3^-]$, $[SO_4^{2-}]$, and $[NH_4^+]$ ions primarily reflect changes in atmospheric circulation, a scenario that is supported by the significant correlations between ion concentrations and large-scale climate indices (Figures 8–10), which we discuss in the following section.

4.3. Contrasting Responses in Neighboring Ice Cores

Ions in the TB and ER cores exhibit opposite correlations with the NAO_{5yr} (Figures 8 and 9). In addition, the ions in the ER and DP cores show similar tendencies. Despite the correlations being weak or nonsignificant, these ions also show contrasting relationships with the other climate indices (Figure 8), whereas anthropogenic emissions from Europe and India South Asia show no such disparities (Figure S4 in Supporting Information S1). Together, these findings suggest that the contrasting correlations among the ice cores reflect atmospheric transport rather than pollution variability. To elucidate the climatic variables potentially driving these contrasting responses (Hersbach et al., 2020), we conducted composite analyses using the ERA5 reanalysis data set. For positive and negative NAO and SOI years ($|\sigma| > 1$; Table S8 in Supporting Information S1), we created composite anomalies of 2-m temperature, wind components, precipitation, and surface air pressure. Figures S5–S10 in Supporting Information S1 show the positive (left column) and negative (right column) years along with their difference (positive minus negative; center column), which are normalized by the interannual standard deviation of each variable. Annual and seasonal values are depicted against the NAO (Figures S5–S7 in Supporting Information S1) and SOI (Figures S8–S10 in Supporting Information S1). For our seasonal assessment, we define winter as the months December–February (DJF), spring as March–May (MAM), summer as June-August (JJA), and autumn as September–November (SON).

Composite anomalies for temperature and precipitation show no spatial variability that can be linked to the contrasting responses between the ice core records. Nonetheless, we did observe a strong negative relationship between the MAM surface pressure anomaly and NAO (Figure 11a). Furthermore, although $[NH_4^+]$ is the sole ion exhibiting moderately significant correlations with SOI_{5yr} (Figure 8), the composite anomalies of springtime surface pressure also show a contrasting pattern with SOI (Figure 11b). We note that the relationship between local climate parameters and the NAO or SOI appear to be opposite; this pattern can explain the opposite responses of TB and ER (and DP) ions to the NAO and SOI (Figure 8), although the spatial anomalies are weak. In other words, we presume that heterogeneity in the spatial distribution of springtime surface pressure, and thus in wind, on both sides of the Himalayas influences the transport of aerosols to each core site, resulting in different responses to the NAO and SOI. The source of $[NH_4^+]$ is thought to be biomass burning, agricultural activities, and energy consumptions in the Indian plains (Kang et al., 2002b), although it remains unclear as to why $[NH_4^+]$ alone correlates with SOI, whereas multiple ions exhibit significant correlations with NAO.

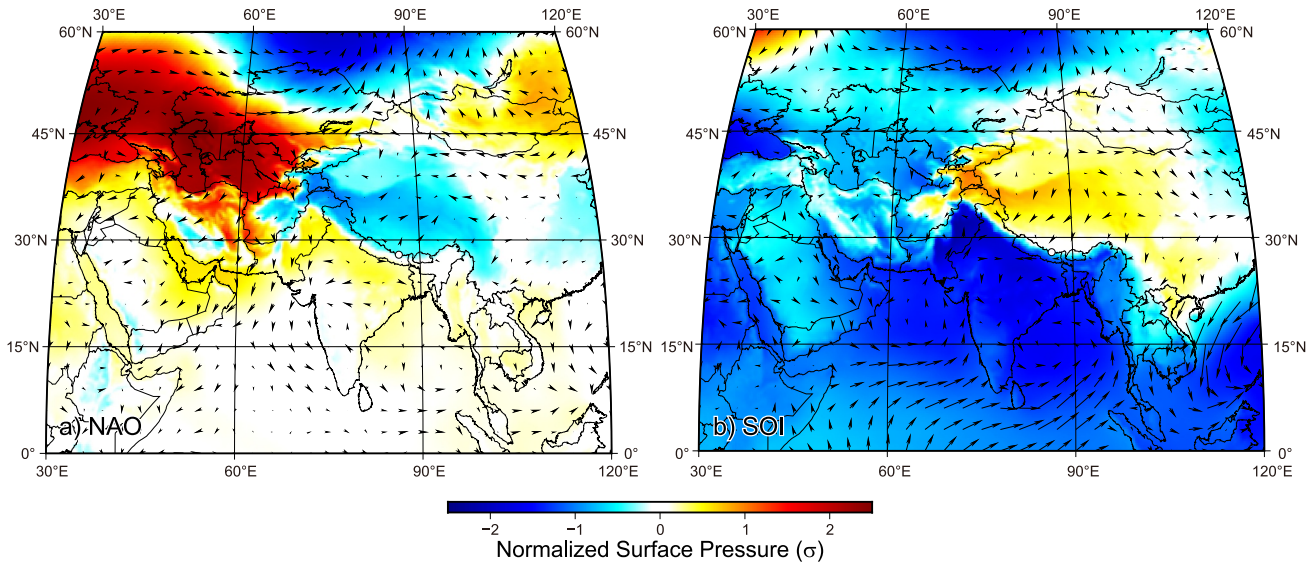

Figure 11. Difference between composite anomalies of positive and negative years of the surface pressure (color scale) and wind (vector) for the spring season (MAM: March, April, May) in the ERA5 reanalysis data for (a) NAO and (b) SOI indices.

Our analysis suggested that spring could be the key season for the contrasting responses in the ice cores. This is consistent with the intense spring atmospheric pollution episode observed by a sun photometer at the Nam Co station in the central Tibetan Plateau (Xia et al., 2011). Spring is the driest season and thus it is unlikely that the ion species are being delivered with precipitation while the contrast of the water stable isotopes among the sites (ER and DP) were analyzed with the precipitation seasonality (Pang et al., 2014). Hu et al. (2022) demonstrated the impact of the Tibetan Plateau on the relationships between aerosols and atmospheric circulation patterns. Their study supports ours though many stations are located at lower elevations than 5,000 m a.s.l. The consistent responses of the ER and DP cores, both from the northern side of the Himalayan range, also support the influence of the Himalayas on atmospheric circulations. However, atmospheric models or reanalysis data might be difficult to describe the contrasting responses because the spatial and topographical resolutions do not sufficiently resolve the Himalayan range at high elevations.

5. Conclusions

In this study, we analyzed concentrations of soluble ions in an ice core recovered from the southern side of the Himalayas. In constructing our core chronology, we applied a protocol that uses $[NO_3^-]$ and $[Ca^{2+}]$ to eliminate subjective bias as much as possible, thus resulting in a record dating back to 1875 CE (with an error of ±2 years). Comparison with a neighboring ice core obtained from the northern side of the Himalayas revealed that the respective variability in ion components is significantly different despite the two core sites being located only 40 km apart. Composite analysis of the ERA5 reanalysis climate data revealed that the spring season is characterized by contrasting atmospheric pressure patterns on the two sides of the Himalayas, thus providing a plausible explanation for the contrasting relationships between ice core chemistry and climate at the two sites with climate indices such as the NAO and SOI. Previous studies have reported disparate accumulation trends among Himalayan ice cores. Our study substantiates this pattern, thereby reinforcing the importance of collecting, analyzing, and comparing multiple ice cores from neighboring sites throughout the Himalayas.

Data Availability Statement

Ion data of the TB core are available at https://doi.org/10.5281/zenodo.14252245 (Tsushima & Fujita, 2024). The ion data of the ER and DP cores are available at National Centers for Environmental Information (NCEI), National Oceanic and Atmospheric Administration (NOAA) (https://www.ncei.noaa.gov/access/paleo-search/study/2469 for ER, and https://www.ncei.noaa.gov/access/paleo-search/study/11180 for DP, last access: 28 Nov. 2024).

The ERA5 reanalysis data are obtained from Copernicus Climate Data Store (https://cds.climate.copernicus.eu/, last access: 28 Nov. 2024). Climate indices were obtained from NOAA site (https://psl.noaa.gov/data/timeseries/month/, last access: 31 Aug. 2024).

Acknowledgments
The authors would thank members of the 2019 drilling team. The authors also appreciate T. Saito, A. Watari, and M. Otsuka for supporting the ice core processing in the cold rooms of the Institute of Low Temperature Science, Hokkaido University, Japan. This study is supported by JSPS-KAKENHI (Grants 17H01621, 18H05292, 22H00033, and 23H00511), Arctic Challenge for Sustainability (ArCS II) Project (Grant JPMXD1420318865), Joint Research Program of Institute of Low Temperature Science, Hokkaido University (Grants 20G047, 21G034, 22G029, and 23G053), General Collaboration Project of National Institute of Polar Research (Grant 3-8 and 30-14), and Global Environmental Research Coordination System of Ministry of the Environment of Japan (Grants MLIT1753 and MLIT2253). The authors would thank H. Pang and an anonymous reviewer for their valuable inputs and reviews.

References

Aizen, E. M., Aizen, V. B., Takeuchi, N., Mayewski, P. A., Grigholm, B., Joswiak, D. R., et al. (2016). Abrupt and moderate climate changes in the mid-latitudes of Asia during the Holocene. *Journal of Glaciology*, *62*(233), 411–439. https://doi.org/10.1017/jog.2016.34

Allan, R. J., Nicholls, N., Jones, P. D., & Butterworth, I. J. (1991). A further extension of the Tahiti-Darwin SOI, early ENSO events and Darwin pressure. *Journal of Climate*, *4*(7), 743–749. https://doi.org/10.1175/1520-0442(1991)004%3C0743:AFEOTT%3E2.0.CO;2

Ashok, K., Guan, Z., & Yamagata, T. (2001). Impact of the Indian Ocean dipole on the relationship between the Indian monsoon rainfall and ENSO. *Geophysical Research Letters*, *28*(23), 4499–4502. https://doi.org/10.1029/2001GL013294

Barnston, A. G., & Livezey, R. E. (1987). Classification, seasonality and persistence of low-frequency atmospheric circulation patterns. *Monthly Weather Review*, *115*(6), 1083–1126. https://doi.org/10.1175/1520-0493(1987)115%3C1083:CSAPOL%3E2.0.CO;2

Brimblecombe, P., Tranter, M., Abrahams, P., Blackwood, I., Davies, T., & Vincent, C. (1985). Relocation and preferential elution of acidic solute through the snowpack of a small, remote, high-altitude Scottish catchment. *Annals of Glaciology*, *7*, 141–147. https://doi.org/10.3189/S0260305500006066

Chen, W. Y., & van den Dool, H. M. (2003). Sensitivity of teleconnection patterns to the sign of their primary action center. *Monthly Weather Review*, *131*(11), 2885–2899. https://doi.org/10.1175/1520-0493(2003)131%3C2885:SOTPTT%3E2.0.CO;2

Chylek, P., Folland, C., Frankcombe, L., Dijkstra, H., Lesins, G., & Dubey, M. (2012). Greenland ice core evidence for spatial and temporal variability of the Atlantic Multidecadal Oscillation. *Geophysical Research Letters*, *39*(9), L09705. https://doi.org/10.1029/2012GL051241

Davis, M. E., Thompson, L. G., Yao, T., & Wang, N. (2005). Forcing of the Asian monsoon on the Tibetan Plateau: Evidence from high-resolution ice core and tropical coral records. *Journal of Geophysical Research*, *110*(D4), D04101. https://doi.org/10.1029/2004JD004933

Delmas, R., & Boutron, C. (1978). Sulfate in Antarctic snow: Spatio-temporal distribution. In *Sulfur in the atmosphere* (pp. 723–728). Elsevier. https://doi.org/10.1016/B978-0-08-022932-4.50075-6

Duan, K., Thompson, L. G., Yao, T., Davis, M. E., & Mosley-Thompson, E. (2007). A 1000 year history of atmospheric sulfate concentrations in southern Asia as recorded by a Himalayan ice core. *Geophysical Research Letters*, *34*(1), L01810. https://doi.org/10.1029/2006GL027456

Enfield, D. B., Mestas-Nuñez, A. M., & Trimble, P. J. (2001). The Atlantic multidecadal oscillation and its relation to rainfall and river flows in the continental US. *Geophysical Research Letters*, *28*(10), 2077–2080. https://doi.org/10.1029/2000GL012745

Farinotti, D., Huss, M., Fürst, J. J., Landmann, J., Machguth, H., Maussion, F., & Pandit, A. (2019). A consensus estimate for the ice thickness distribution of all glaciers on Earth. *Nature Geoscience*, *12*(3), 168–173. https://doi.org/10.1038/s41561-019-0300-3

Gong, D.-Y., Yang, J., Kim, S.-J., Gao, Y., Guo, D., Zhou, T., & Hu, M. (2011). Spring Arctic Oscillation-East Asian summer monsoon connection through circulation changes over the western North Pacific. *Climate Dynamics*, *37*(11–12), 2199–2216. https://doi.org/10.1007/s00382-011-1041-1

Grigholm, B., Mayewski, P. A., Kang, S., Zhang, Y., Kaspari, S., Sneed, S. B., & Zhang, Q. (2009). Atmospheric soluble dust records from a Tibetan ice core: Possible climate proxies and teleconnection with the Pacific Decadal Oscillation. *Journal of Geophysical Research*, *114*(D20), D20118. https://doi.org/10.1029/2008JD011242

Hammer, C. U. (1980). Acidity of polar ice cores in relation to absolute dating, past volcanism, and radio–echoes. *Journal of Glaciology*, *25*(93), 359–372. https://doi.org/10.3189/S0022143000015227

Hersbach, H., Bell, B., Berrisford, P., Hirahara, S., Horányi, A., Muñoz-Sabater, J., et al. (2020). The ERA5 global reanalysis. *Quarterly Journal of the Royal Meteorological Society*, *146*(730), 1999–2049. https://doi.org/10.1002/qj.3803

Hoesly, R. M., Smith, S. J., Feng, L., Klimont, Z., Janssens-Maenhout, G., Pitkanen, T., et al. (2018). Historical (1750–2014) anthropogenic emissions of reactive gases and aerosols from the Community Emissions Data System (CEDS). *Geoscientific Model Development*, *11*(1), 369–408. https://doi.org/10.5194/gmd-11-369-2018

Hou, S., Jenk, T. M., Zhang, W., Wang, C., Wu, S., Wang, Y., et al. (2018). Age ranges of the Tibetan ice cores with emphasis on the Chongce ice cores, western Kunlun Mountains. *The Cryosphere*, *12*(7), 2341–2348. https://doi.org/10.5194/tc-12-2341-2018

Hou, S., Qin, D., Zhang, D., Kang, S., Mayewski, P. A., & Wake, C. P. (2003). A 154a high-resolution ammonium record from the Rongbuk Glacier, north slope of Mt. Qomolangma (Everest), Tibet–Himal region. *Atmospheric Environment*, *37*(5), 721–729. https://doi.org/10.1016/S1352-2310(02)00582-4

Hou, S., Zhang, W., Pang, H., Wu, S.-Y., Jenk, T. M., Schwikowski, M., & Wang, Y. (2019). Apparent discrepancy of Tibetan ice core $\delta^{18}O$ records may be attributed to misinterpretation of chronology. *The Cryosphere*, *13*(6), 1743–1752. https://doi.org/10.5194/tc-13-1743-2019

Hu, Y., Kang, S., Yang, J., Ji, Z., Rupakheti, D., Yin, X., & Du, H. (2022). Impact of atmospheric circulation patterns on properties and regional transport pathways of aerosols over Central-West Asia: Emphasizing the Tibetan Plateau. *Atmospheric Research*, *266*, 105975. https://doi.org/10.1016/j.atmosres.2021.105975

Iizuka, Y., Uemura, R., Fujita, K., Hattori, S., Seki, O., Miyamoto, C., et al. (2018). A 60 year record of atmospheric aerosol depositions preserved in a high-accumulation dome ice core, Southeast Greenland. *Journal of Geophysical Research: Atmospheres*, *123*(1), 574–589. https://doi.org/10.1002/2017JD026733

Joswiak, D. R., Yao, T., Wu, G., Tian, L., & Xu, B. (2013). Ice-core evidence of westerly and monsoon moisture contributions in the central Tibetan Plateau. *Journal of Glaciology*, *59*(213), 56–66. https://doi.org/10.3189/2013JoG12J035

Kang, S., Mayewski, P. A., Qin, D., Sneed, S. A., Ren, J., & Zhang, D. (2004). Seasonal differences in snow chemistry from the vicinity of Mt. Everest, central Himalayas. *Atmospheric Environment*, *38*(18), 2819–2829. https://doi.org/10.1016/j.atmosenv.2004.02.043

Kang, S., Mayewski, P. A., Qin, D., Yan, Y., Hou, S., Zhang, D., et al. (2002a). Glaciochemical records from a Mt. Everest ice core: Relationship to atmospheric circulation over Asia. *Atmospheric Environment*, *36*(21), 3351–3361. https://doi.org/10.1016/S1352-2310(02)00325-4

Kang, S., Mayewski, P. A., Qin, D., Yan, Y., Zhang, D., Hou, S., & Ren, J. (2002b). Twentieth century increase of atmospheric ammonia recorded in Mount Everest ice core. *Journal of Geophysical Research*, *107*(D21), 4595. https://doi.org/10.1029/2001JD001413

Kaspari, S., Hooke, R. L., Mayewski, P. A., Kang, S., Hou, S., & Qin, D. (2008). Snow accumulation rate on Qomolangma (Mount Everest), Himalaya: Synchroneity with sites across the Tibetan Plateau on 50–100 year timescales. *Journal of Glaciology*, *54*(185), 343–352. https://doi.org/10.3189/002214308784886126

Kaspari, S., Mayewski, P. A., Kang, S., Sneed, S. A., Hou, S., Hooke, R., et al. (2007). Reduction in northward incursions of the South Asian monsoon since 1400 AD inferred from a Mt. Everest ice core. *Geophysical Research Letters*, *34*(16), L16701. https://doi.org/10.1029/2007GL030440

Keene, W. C., Pszenny, A. A., Galloway, J. N., & Hawley, M. E. (1986). Sea-salt corrections and interpretation of constituent ratios in marine precipitation. *Journal of Geophysical Research*, *91*(D6), 6647–6658. https://doi.org/10.1029/JD091iD06p06647

Können, G. P., Jones, P. D., Kaltofen, M., & Allan, R. J. (1998). Pre-1866 extensions of the Southern Oscillation Index using early Indonesian and Tahitian meteorological readings. *Journal of Climate*, *11*(9), 2325–2339. https://doi.org/10.1175/1520-0442(1998)011%3C2325:PEOTSO%3E2.0.CO;2

Kumar, S., & Raman, R. S. (2016). Inorganic ions in ambient fine particles over a National Park in central India: Seasonality, dependencies between $SO^{14\ 2-}$, $NO^{3\ -}$, and $NH^{14\ +}$, and neutralization of aerosol acidity. *Atmospheric Environment*, *143*, 152–163. https://doi.org/10.1016/j.atmosenv.2016.08.037

Legrand, M., & Mayewski, P. (1997). Glaciochemistry of polar ice cores: A review. *Reviews of Geophysics*, *35*(3), 219–243. https://doi.org/10.1029/96RG03527

Moore, G. K., Holdsworth, G., & Alverson, K. (2002). Climate change in the North Pacific region over the past three centuries. *Nature*, *420*(6914), 401–403. https://doi.org/10.1038/nature01229

Okamoto, S., Fujita, K., Narita, H., Uetake, J., Takeuchi, N., Miyake, T., et al. (2011). Reevaluation of the reconstruction of summer temperatures from melt features in Belukha ice cores, Siberian Altai. *Journal of Geophysical Research*, *116*(D2), D02110. https://doi.org/10.1029/2010JD013977

Olivier, S., Blaser, C., Brütsch, S., Frolova, N., Gäggeler, H., Henderson, K., et al. (2006). Temporal variations of mineral dust, biogenic tracers, and anthropogenic species during the past two centuries from Belukha ice core, Siberian Altai. *Journal of Geophysical Research*, *111*(D5), D05309. https://doi.org/10.1029/2005JD005830

Pang, H., He, Y., Hou, S., & Zhang, N. (2012). Changes in ionic and oxygen isotopic composition of the snow-firn pack at Baishui Glacier No. 1, southeastern Tibetan Plateau. *Environmental Earth Sciences*, *67*(8), 2345–2358. https://doi.org/10.1007/s12665-012-1681-4

Pang, H., He, Y., Theakstone, W. H., & Zhang, D. D. (2007). Soluble ionic and oxygen isotopic compositions of a shallow firn profile, Baishui glacier No. 1, southeastern Tibetan Plateau. *Annals of Glaciology*, *46*, 325–330. https://doi.org/10.3189/172756407782871648

Pang, H., Hou, S., Kaspari, S., & Mayewski, P. A. (2014). Influence of regional precipitation patterns on stable isotopes in ice cores from the central Himalayas. *The Cryosphere*, *8*(1), 289–301. https://doi.org/10.5194/tc-8-289-2014

Qin, D., Hou, S., Zhang, D., Ren, J., Kang, S., Mayewski, P. A., & Wake, C. P. (2002). Preliminary results from the chemical records of an 80.4 m ice core recovered from East Rongbuk Glacier, Qomolangma (Mount Everest), Himalaya. *Annals of Glaciology*, *35*, 278–284. https://doi.org/10.3189/172756402781816799

Rampino, M. R., & Self, S. (1982). Historic eruptions of Tambora (1815), Krakatau (1883), and Agung (1963), their stratospheric aerosols, and climatic impact. *Quaternary Research*, *18*(2), 127–143. https://doi.org/10.1016/0033-5894(82)90065-5

Saji, N., & Yamagata, T. (2003). Possible impacts of Indian Ocean Dipole mode events on global climate. *Climate Research*, *25*(2), 151–169. https://doi.org/10.3354/cr025151

Smith, S. J., Pitcher, H., & Wigley, T. M. (2001). Global and regional anthropogenic sulfur dioxide emissions. *Global and Planetary Change*, *29*(1–2), 99–119. https://doi.org/10.1016/S0921-8181(00)00057-6

Sunako, S., Fujita, K., Sakai, A., & Kayastha, R. B. (2019). Mass balance of Trambau Glacier, Rolwaling region, Nepal Himalaya: In-situ observations, long-term reconstruction and mass-balance sensitivity. *Journal of Glaciology*, *65*(252), 605–616. https://doi.org/10.1017/jog.2019.37

Takeuchi, N., Hori, Y., Furukawa, N., Yoshida, M., & Fujii, Y. (2020). Glacio-environmental aspects recorded in two shallow ice cores drilled in 1980 at accumulation area of Khumbu Glacier of Mt. Everest in Nepal Himalayas. *Arctic Antarctic and Alpine Research*, *52*(1), 605–616. https://doi.org/10.1080/15230430.2020.1833681

Thompson, L. G., Yao, T., Mosley-Thompson, E., Davis, M. E., Henderson, K., & Lin, P.-N. (2000). A high-resolution millennial record of the South Asian monsoon from Himalayan ice cores. *Science*, *289*(5486), 1916–1919. https://doi.org/10.1126/science.289.5486.1916

Tian, R., & Tian, L. (2019). Two decades ammonium records from ice core in Qiangyong glacier in the Northern Himalayas. *Atmospheric Research*, *222*, 36–46. https://doi.org/10.1016/j.atmosres.2019.02.004

Tripathee, L., Kang, S., Rupakheti, D., Cong, Z., Zhang, Q., & Huang, J. (2017). Chemical characteristics of soluble aerosols over the central Himalayas: Insights into spatiotemporal variations and sources. *Environmental Science and Pollution Research*, *24*(31), 24454–24472. https://doi.org/10.1007/s11356-017-0077-0

Tsushima, A., & Fujita, K. (2024). *Major ions in Trambau ice core, Nepal Himalaya*. Zenodo. https://doi.org/10.5281/zenodo.14252245

Tsushima, A., Miyahara, M., Yamasaki, T., Esashi, N., Sato, Y., Kayastha, R. B., et al. (2021). Ice core drilling on a high-elevation accumulation zone of Trambau Glacier in the Nepal Himalaya. *Annals of Glaciology*, *62*(85–86), 353–359. https://doi.org/10.1017/aog.2021.15

van den Dool, H., Saha, S., & Johansson, Å. (2000). Empirical orthogonal teleconnections. *Journal of Climate*, *13*(8), 1421–1435. https://doi.org/10.1175/1520-0442(2000)013%3C1421:EOT%3E2.0.CO;2

Virkkunen, K., Moore, J., Isaksson, E., Pohjola, V., Perämäki, P., Grinsted, A., & Kekonen, T. (2007). Warm summers and ion concentrations in snow: Comparison of present day with Medieval Warm Epoch from snow pits and an ice core from Lomonosovfonna, Svalbard. *Journal of Glaciology*, *53*(183), 623–634. https://doi.org/10.3189/002214307784409388

Wang, C., Dong, S., Evan, A. T., Foltz, G. R., & Lee, S.-K. (2012). Multidecadal covariability of North Atlantic sea surface temperature, African dust, Sahel rainfall, and Atlantic hurricanes. *Journal of Climate*, *25*(15), 5404–5415. https://doi.org/10.1175/JCLI-D-11-00413.1

Wang, N., Thompson, L. G., Davis, M. E., Mosley-Thompson, E., Yao, T., & Pu, J. (2003). Influence of variations in NAO and SO on air temperature over the northern Tibetan Plateau as recorded by $\delta^{18}O$ in the Malan ice core. *Geophysical Research Letters*, *30*(22), 2167. https://doi.org/10.1029/2003GL018188

Wang, N., Yao, T., Thompson, L. G., & Davis, M. E. (2002). Indian monsoon and North Atlantic Oscillation signals reflected by Cl-and Na^+ in a shallow ice core from Dasuopu glacier, Xixabangma, Himalaya. *Annals of Glaciology*, *35*, 273–277. https://doi.org/10.3189/172756402781816825

Webster, P. J., & Yang, S. (1992). Monsoon and ENSO: Selectively interactive systems. *Quarterly Journal of the Royal Meteorological Society*, *118*(507), 877–926. https://doi.org/10.1002/qj.49711850705

Xia, X., Zong, X., Cong, Z., Chen, H., Kang, S., & Wang, P. (2011). Baseline continental aerosol over the central Tibetan plateau and a case study of aerosol transport from South Asia. *Atmospheric Environment*, *45*(39), 7370–7378. https://doi.org/10.1016/j.atmosenv.2011.07.067

Xu, H., Hou, S., Pang, H., & Wang, C. (2016). Effects of ENSO on the major ion record of a Qomolangma (Mount Everest) ice core. *Annals of Glaciology*, *57*(71), 282–288. https://doi.org/10.3189/2016AoG71A042

Xu, J., Hou, S., Qin, D., Kang, S., Ren, J., & Ming, J. (2007). Dust storm activity over the Tibetan Plateau recorded by a shallow ice core from the north slope of Mt. Qomolangma (Everest), Tibet-Himal region. *Geophysical Research Letters*, *34*(17), L17504. https://doi.org/10.1029/2007GL030853

Xu, J., Hou, S., Qin, D., Kaspari, S., Mayewski, P. A., Petit, J. R., et al. (2010). A 108.83-m ice-core record of atmospheric dust deposition at Mt. Qomolangma (Everest), Central Himalaya. *Quaternary Research*, *73*(1), 33–38. https://doi.org/10.1016/j.yqres.2009.09.005

Xu, J., Kaspari, S., Hou, S., Kang, S., Qin, D., Ren, J., & Mayewski, P. A. (2009). Records of volcanic events since AD 1800 in the East Rongbuk ice core from Mt. Qomolangma. *Chinese Science Bulletin*, *54*(8), 1411–1416. https://doi.org/10.1007/s11434-009-0020-y

Yang, D., Yao, T., Wu, G., Zhu, M., Zhao, H., Shi, Y., & Qu, D. (2022). Different patterns and origins between northwestern and southeastern Tibetan ice core glaciochemical records over the past century. *Science of the Total Environment*, *819*, 153195. https://doi.org/10.1016/j.scitotenv.2022.153195

Yang, X., Yao, T., Joswiak, D., & Yao, P. (2014). Integration of Tibetan Plateau ice-core temperature records and the influence of atmospheric circulation on isotopic signals in the past century. *Quaternary Research*, *81*(3), 520–530. https://doi.org/10.1016/j.yqres.2014.01.006

Yao, T., Duan, K., Xu, B., Wang, N., Guo, X., & Yang, X. (2008). Precipitation record since AD 1600 from ice cores on the central Tibetan Plateau. *Climate of the Past*, *4*(3), 175–180. https://doi.org/10.5194/cp-4-175-2008

Zhang, W., Hou, S., Liu, Y., Wu, S., An, W., Pang, H., & Wang, C. (2017). A high-resolution atmospheric dust record for 1810–2004 AD derived from an ice core in eastern Tien Shan, central Asia. *Journal of Geophysical Research: Atmospheres*, *122*(14), 7505–7518. https://doi.org/10.1002/2017JD026699

Zhang, Y., Kang, S., Zhang, Q., Grigholm, B., Kaspari, S., You, Q., et al. (2015). A 500 year atmospheric dust deposition retrieved from a Mt. Geladaindong ice core in the central Tibetan Plateau. *Atmospheric Research*, *166*, 1–9. https://doi.org/10.1016/j.atmosres.2015.06.007

Supporting Information for "Contrasting responses of ion concentration variations to atmospheric patterns in central Himalayan ice cores"

Akane Tsushima[1,2], Nao Esashi[3], Sumito Matoba[4], Yoshinori Iizuka[4], Ryu Uemura[3], Kouji Adachi[5], Takeshi Kinase[5,6], Motohiro Hirabayashi[7], Kaoru Kawakami[4], Rijan B. Kayastha[8], and Koji Fujita[3]

[1]Graduate School of Science, Chiba University, Chiba, Japan

[2]Now at Graduate School of Integrated Science and Technology, Nagasaki University, Nagasaki, Japan

[3]Graduate School of Environmental Studies, Nagoya University, Nagoya, Japan

[4]Institute of Low Temperature Science, Hokkaido University, Sapporo, Japan

[5]Meteorological Research Institute, Tsukuba, Japan

[6]Japan Agency for Marine-Earth Science and Technology (JAMSTEC), Yokohama, Japan

[7]National Institute of Polar Research, Tokyo, Japan

[8]Himalayan Cryosphere, Climate and Disaster Research Center, Department of Environmental Science and Engineering, School of Science, Kathmandu University, Dhulikhel, Nepal

Contents of this file

1. Tables S1 to S8
2. Figures S1 to S10

0148-0227/24/$9.00

Table S1. Correlation coefficients among annual mean of major ions in the TB core (Figure 7a).

	$[Na^+]$	$[Cl^-]$	$[NH_4^+]$	$[K^+]$	$[Mg^{2+}]$	$[Ca^{2+}]$	$[NO_3^-]$	$[SO_4^{2-}]$
$[Na^+]$	1.000	–	–	–	–	–	–	–
$[Cl^-]$	0.845	1.000	–	–	–	–	–	–
$[NH_4^+]$	$0.189^{\#}$	0.493	1.000	–	–	–	–	–
$[K^+]$	0.481	0.290	$0.202^{\#}$	1.000	–	–	–	–
$[Mg^{2+}]$	0.308	0.259*	0.283	0.594	1.000	–	–	–
$[Ca^{2+}]$	0.660	0.443	$0.195^{\#}$	0.808	0.668	1.000	–	–
$[NO_3^-]$	0.665	0.438	0.129^{+}	0.733	0.587	0.881	1.000	–
$[SO_4^{2-}]$	0.693	0.363	0.010^{+}	0.731	0.487	0.880	0.872	1.000

$^{+}$ $p > 0.05$, $^{\#}$ $0.05 > p > 0.01$, * $0.01 > p > 0.001$, no remark $p < 0.001$

Table S2. Same as Table S1 but for the ER core (Figure 7b).

	$[Na^+]$	$[Cl^-]$	$[NH_4^+]$	$[K^+]$	$[Mg^{2+}]$	$[Ca^{2+}]$	$[NO_3^-]$	$[SO_4^{2-}]$
$[Na^+]$	1.000	–	–	–	–	–	–	–
$[Cl^-]$	0.680	1.000	–	–	–	–	–	–
$[NH_4^+]$	0.362	0.317	1.000	–	–	–	–	–
$[K^+]$	0.631	0.609	0.265*	1.000	–	–	–	–
$[Mg^{2+}]$	0.387	0.145^{+}	0.497	$0.194^{\#}$	1.000	–	–	–
$[Ca^{2+}]$	0.446	0.278*	0.591	0.093^{+}	0.599	1.000	–	–
$[NO_3^-]$	0.605	0.423	0.562	0.235*	0.483	0.792	1.000	–
$[SO_4^{2-}]$	0.400	0.365	0.532	0.251*	0.436	0.662	0.849	1.000

$^{+}$ $p > 0.05$, $^{\#}$ $0.05 > p > 0.01$, * $0.01 > p > 0.001$, no remark $p < 0.001$

Table S3. Correlation coefficients of the major ions in the TB core against NAO, SOI, DMI, and AMO, which are depicted in Figure 8a. Subscript 5yr denotes comparison among the 5-year running means for both ion and index.

	NAO	NAO_{5yr}	SOI	SOI_{5yr}	DMI	DMI_{5yr}	AMO	AMO_{5yr}
$[Na^+]$	-0.019^{+}	0.069^{+}	-0.034^{+}	-0.044^{+}	$0.165^{\#}$	$0.213^{\#}$	$0.184^{\#}$	0.229*
$[Cl^-]$	-0.074^{+}	-0.107^{+}	-0.008^{+}	0.091^{+}	$0.187^{\#}$	0.265*	$0.202^{\#}$	0.255*
$[NH_4^+]$	-0.223^{+}	–0.540	$0.196^{\#}$	0.373	0.053^{+}	$0.185^{\#}$	0.052^{+}	0.073^{+}
$[K^+]$	$-0.240^{\#}$	-0.583^{+}	0.033^{+}	0.124^{+}	-0.047^{+}	-0.126^{+}	-0.037^{+}	-0.017^{+}
$[Mg^{2+}]$	$-0.255^{\#}$	–0.484	0.129^{+}	0.145^{+}	-0.099^{+}	0.025^{+}	0.069^{+}	0.129^{+}
$[Ca^{2+}]$	-0.216^{+}	–0.424	-0.048^{+}	0.001^{+}	-0.062^{+}	-0.112^{+}	0.103^{+}	0.145^{+}
$[NO_3^-]$	-0.169^{+}	-0.212^{+}	-0.025^{+}	0.007^{+}	-0.010^{+}	0.031^{+}	0.145^{+}	0.235*
$[SO_4^{2-}]$	$-0.283^{\#}$	–0.532	-0.030^{+}	0.002^{+}	-0.034^{+}	-0.076^{+}	0.148^{+}	0.218*

$^{+}$ $p > 0.05$, $^{\#}$ $0.05 > p > 0.01$, * $0.01 > p > 0.001$, no remark $p < 0.001$

Table S4. Same as Table S3 but for the ER core (Figure 8b).

	NAO	NAO_{5yr}	SOI	SOI_{5yr}	DMI	DMI_{5yr}	AMO	AMO_{5yr}
$[Na^+]$	0.117^{+}	0.193^{+}	0.012^{+}	-0.070^{+}	-0.171^{+}	-0.307^{+}	0.001^{+}	-0.095^{+}
$[Cl^-]$	0.028^{+}	0.072^{+}	0.010^{+}	0.017^{+}	-0.145^{+}	-0.091^{+}	-0.125^{+}	–0.264*
$[NH_4^+]$	0.199^{+}	0.718	-0.126^{+}	–0.296*	0.152^{+}	0.402	–0.285*	–0.381
$[K^+]$	-0.024^{+}	0.083^{+}	0.068^{+}	0.175^{+}	-0.152^{+}	-0.104^{+}	0.007^{+}	-0.043^{+}
$[Mg^{2+}]$	0.137^{+}	0.507	-0.145^{+}	-0.145^{+}	0.079^{+}	0.084^{+}	-0.105^{+}	$-0.196^{\#}$
$[Ca^{2+}]$	$0.324^{\#}$	0.657	-0.048^{+}	–0.245*	0.099^{+}	0.266*	-0.160^{+}	$-0.231^{\#}$
$[NO_3^-]$	0.373*	0.549	-0.063^{+}	–0.247*	-0.072^{+}	0.091^{+}	-0.160^{+}	–0.305
$[SO_4^{2-}]$	$0.316^{\#}$	0.388*	0.017^{+}	0.018^{+}	-0.064^{+}	$0.198^{\#}$	–0.269*	–0.464

$^{+}$ $p > 0.05$, $^{\#}$ $0.05 > p > 0.01$, * $0.01 > p > 0.001$, no remark $p < 0.001$

Table S5. Same as Table S3 but for the DP core.

	NAO	NAO_{5yr}	SOI	SOI_{5yr}	DMI	DMI_{5yr}	AMO	AMO_{5yr}
$[Cl^-]$	0.276^+	0.743	-0.078^+	–0.327	0.237*	0.467	-0.023^+	-0.020^+
$[NO_3^-]$	0.410*	0.767	–0.273*	–0.424	0.288*	0.470	$-0.185^\#$	–0.261*
$[SO_4^{2-}]$	0.487	0.779	-0.162^+	–0.410	$0.204^\#$	0.429	-0.109^+	-0.160^+

$^+$ $p > 0.05$, $^\#$ $0.05 > p > 0.01$, * $0.01 > p > 0.001$, no remark $p < 0.001$

Table S6. Coefficient of variation (CV) and a ratio of maxima to minima (MXMN) within annual layers for the TB and ER cores.

	CV		MXMN	
	TB	ER	TB	ER
$[Na^+]$	9.6	1.1	4.3	25.0
$[Cl^-]$	11.7	0.8	6.8	9.3
$[NH_4^+]$	29.6	0.6	7.9	5.1
$[K^+]$	6.5	0.9	5.7	16.2
$[Mg^{2+}]$	3.6	0.8	5.3	9.3
$[Ca^{2+}]$	51.6	0.9	7.8	11.0
$[NO_3^-]$	57.5	0.8	9.2	8.4
$[SO_4^{2-}]$	50.0	0.6	9.0	4.5

Table S7. Countries (code: ISO 3166-1 alpha-3) included in the emissions from Europe and South Asia.

Region	n	Country code
Europe	39	ALB, AUT, BEL, BGR, BIH, BLR, CHE, CZE, DEU, DNK, ESP, EST, FIN, FRA, GBR, GRC, HRV, HUN, IRL, ISL, ITA, LIE, LTU, LUX, LVA, MDA, MKD, MLT, MNE, NLD, NOR, POL, PRT, ROU, SRB, SVK, SVN, SWE, UKR
South Asia	6	BGD, BTN, IND, LKA, NPL, PAK

Table S8. Selected years ($|\sigma| > 1$) for the composite anomaly analyses.

	n	Selected year
NAO positive	10	1972, 1982*, 1986, 1989, 1990, 1992*, 1994*, 1999, 2015*, 2018
NAO negative	5	1980, 1998, 2008*, 2010, 2012
SOI positive	5	1971, 1974, 1975, 2008*, 2011
SOI negative	9	1977, 1982*, 1983, 1987, 1992*, 1993, 1994*, 1997, 2015*

* Years overlapping with other indices.

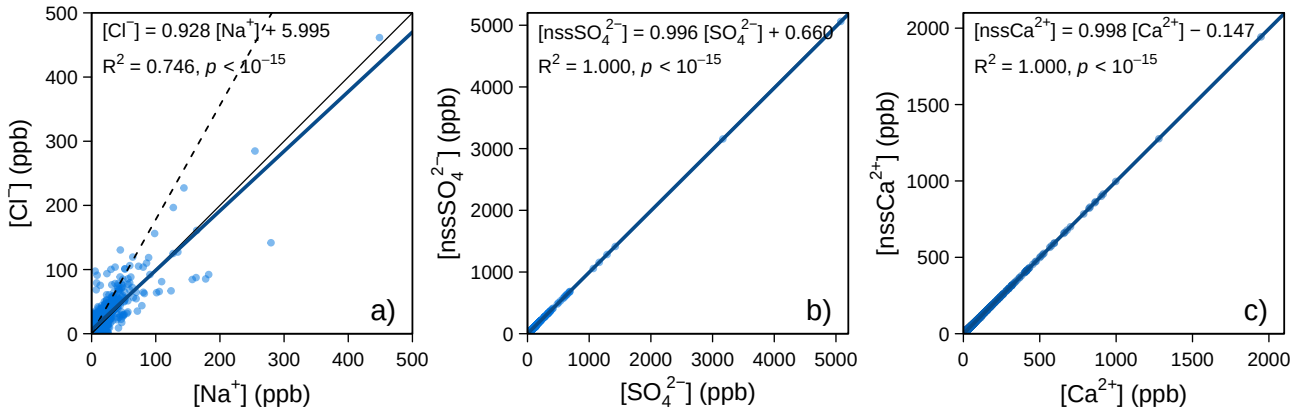

Figure S1. Scatter plots of a) $[Na^+]$ and $[Cl^-]$, b) total and non-sea-salt $[SO_4{}^{2-}]$, and c) total and non-sea-salt $[Ca^{2+}]$ in the TB core. Blue lines denote the linear regressions. Dashed line in panel (a) denotes the sea salt ratio (1.78).

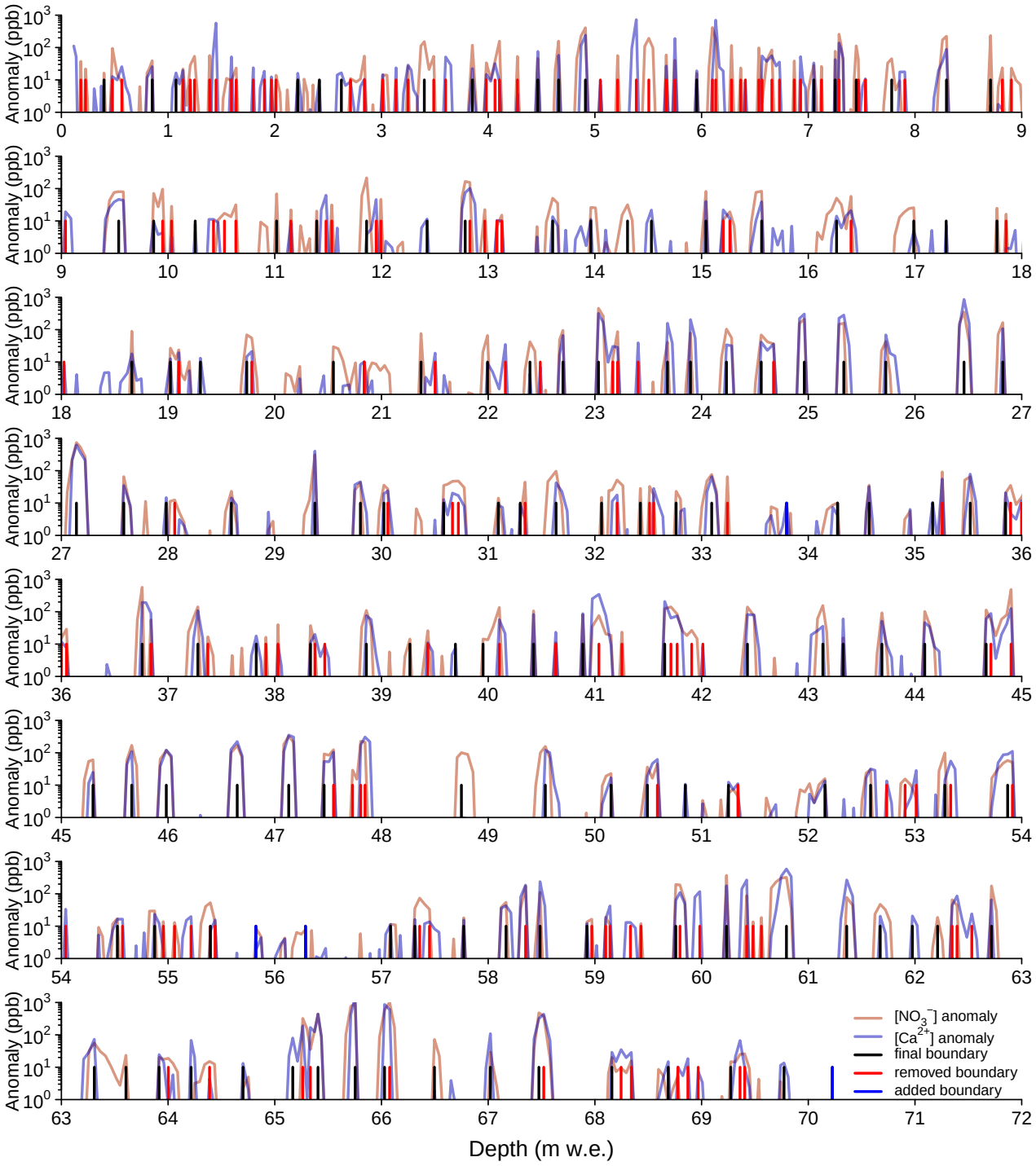

Figure S2. Anomalies of $[NO_3^-]$ and $[Ca^{2+}]$ with the final, removed, and added annual boundaries through the entire core depth.

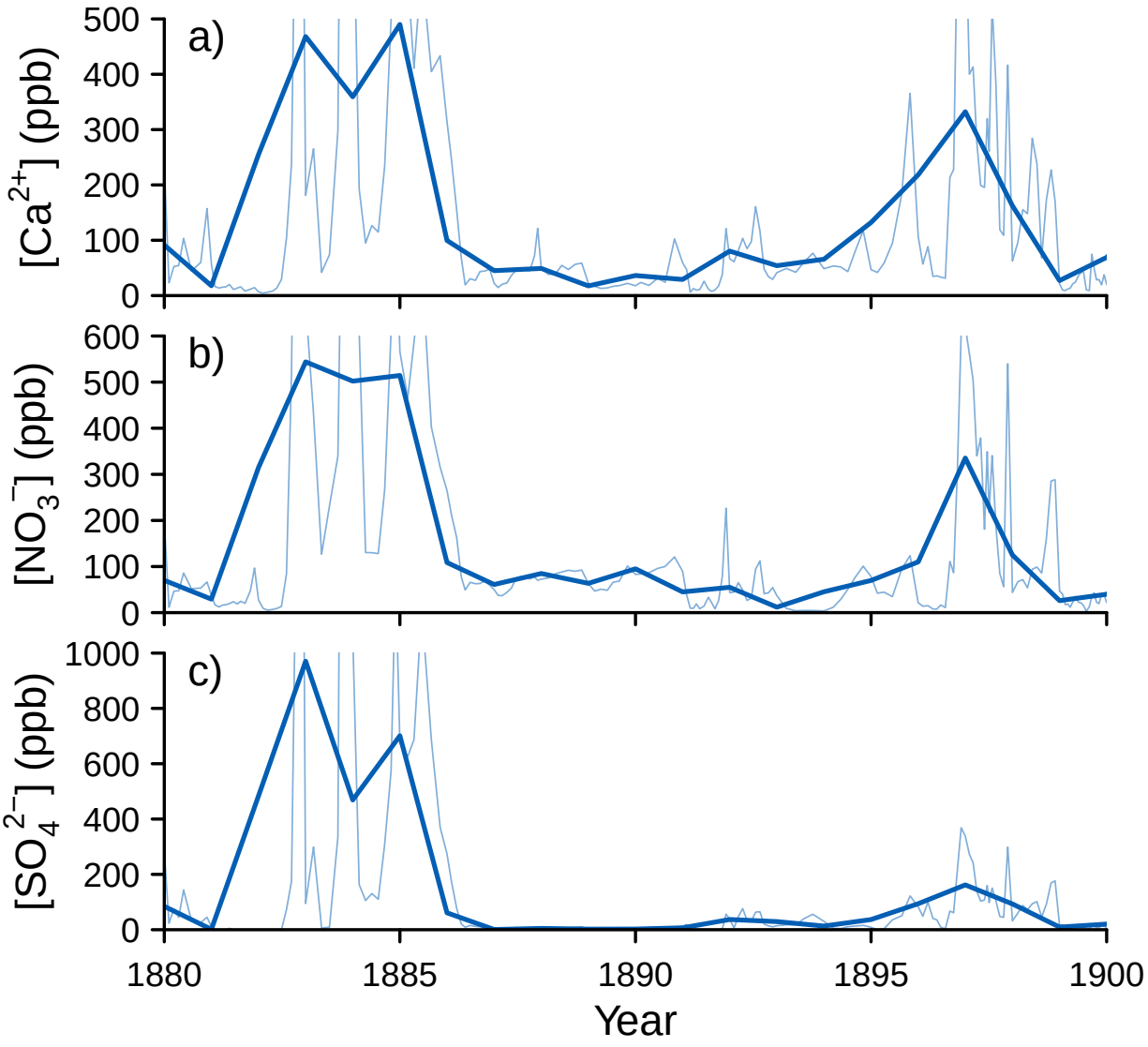

Figure S3. Annual means of a) [Ca^{2+}], b) [NO_3^-], and c) [SO_4^{2-}] ions of the TB core for the period 1880-1900.

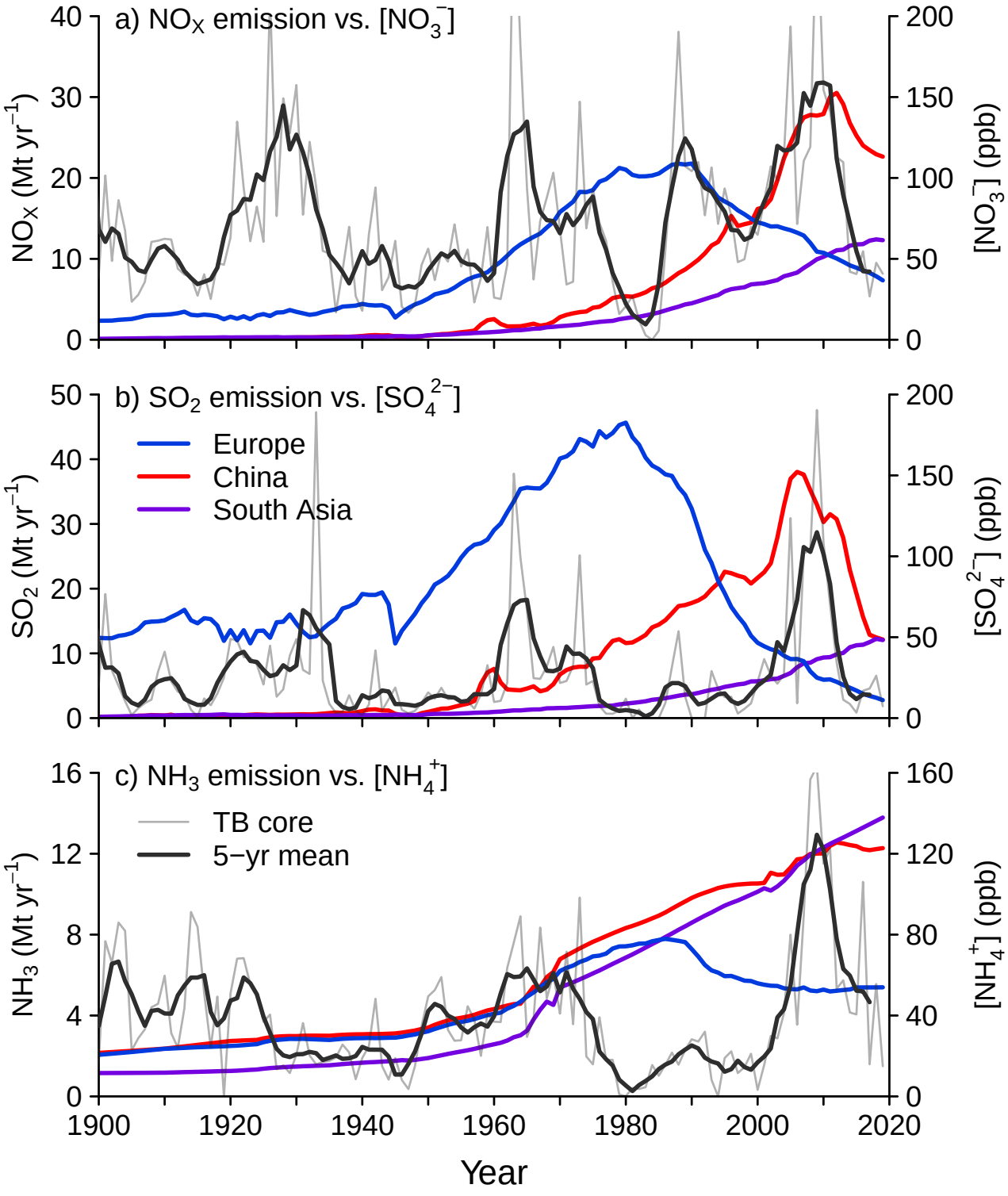

Figure S4. Comparison between regional emissions and the ion concentrations in the TB core. Countries included in Europe and South Asia are listed in Table S7.

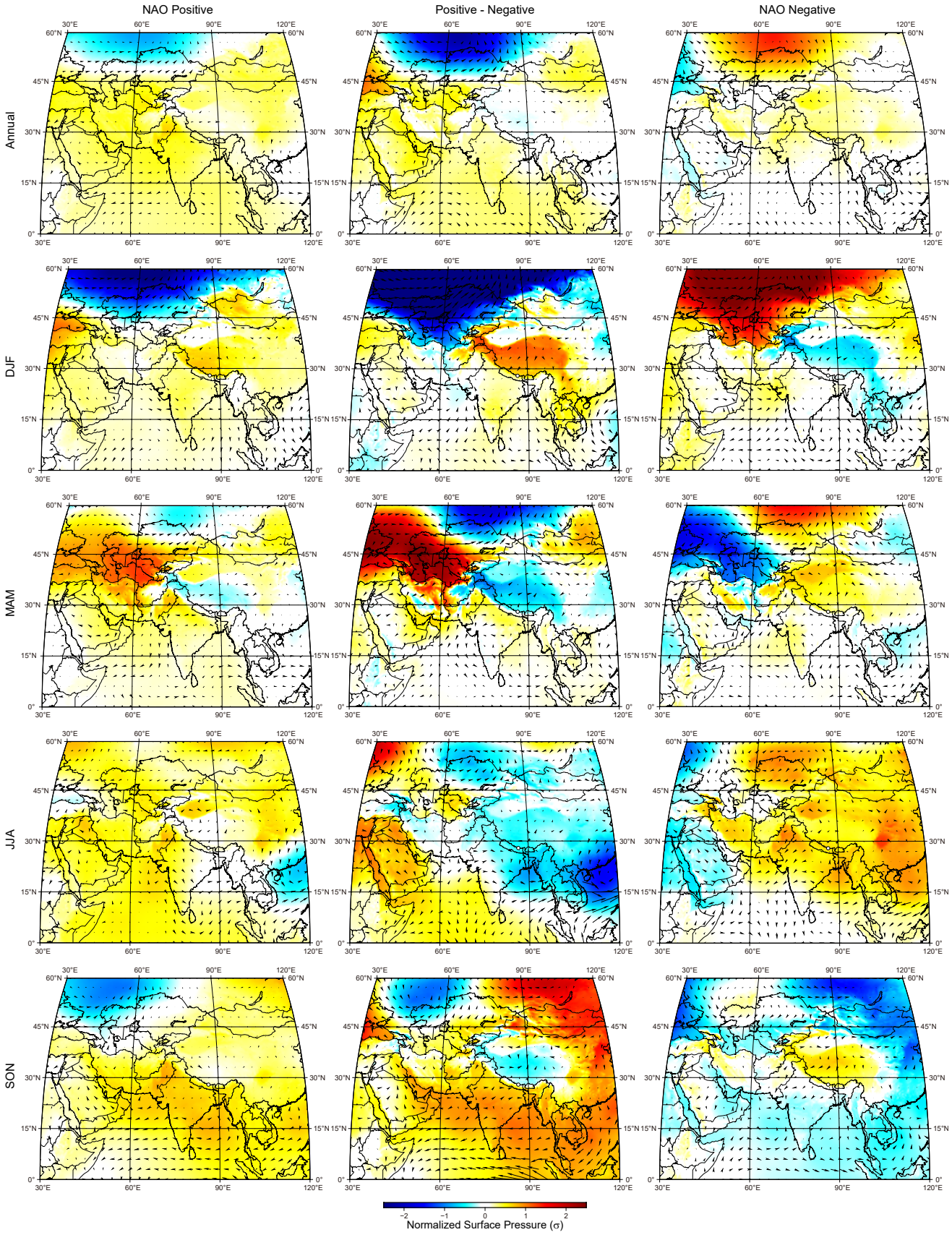

Figure S5. Composite anomalies of surface pressure (color scale) and wind (vector) of the ERA5 reanalysis data for positive (left panels) and negative (right panels) NAO years, and their difference (middle panels). From up to down panels, annual and seasonal (DJF as winter, MAM as spring, JJA as summer, and SON as autumn) are shown.

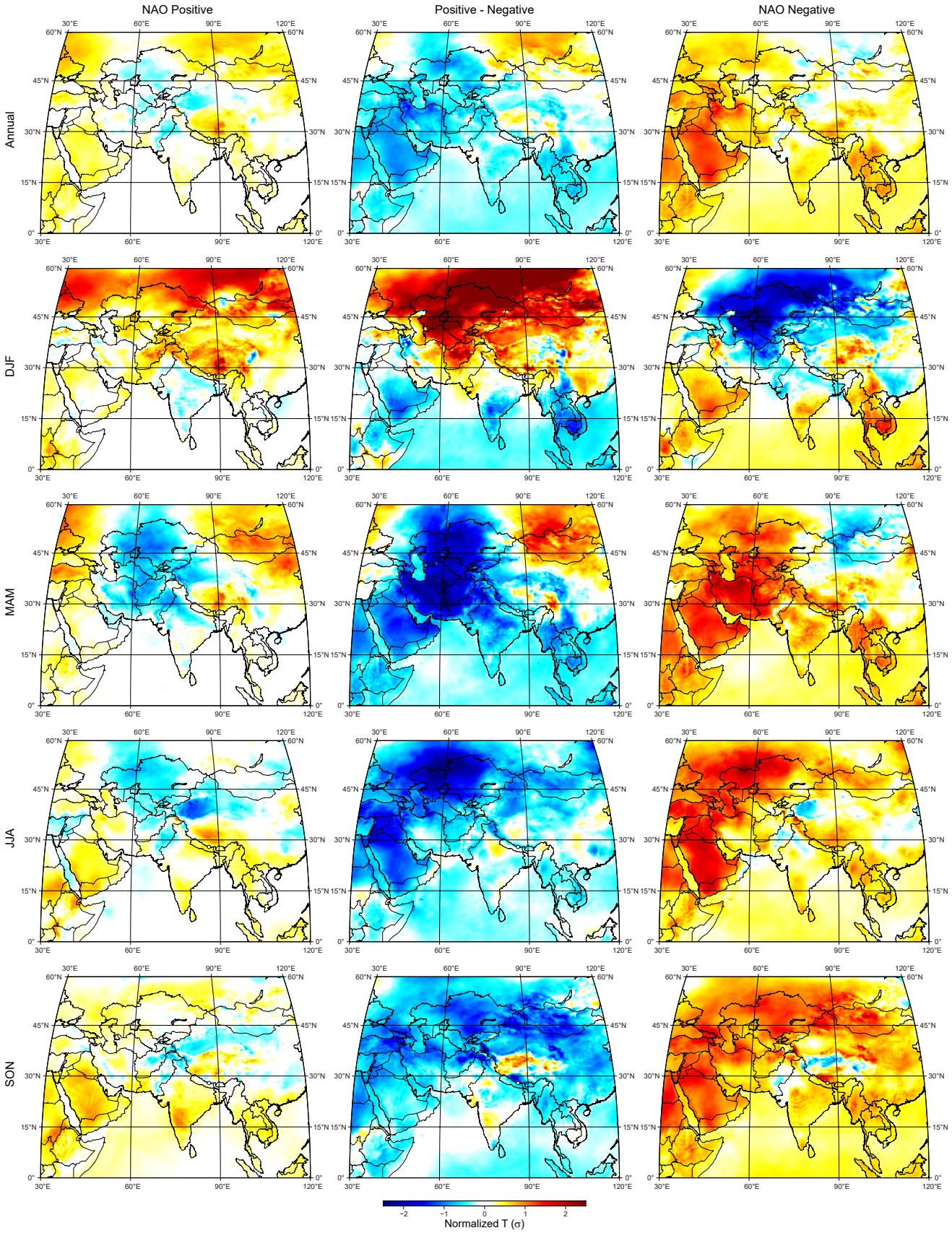

Figure S6. As of Figure S5 but for the ERA5 2-m temperature (color scale).

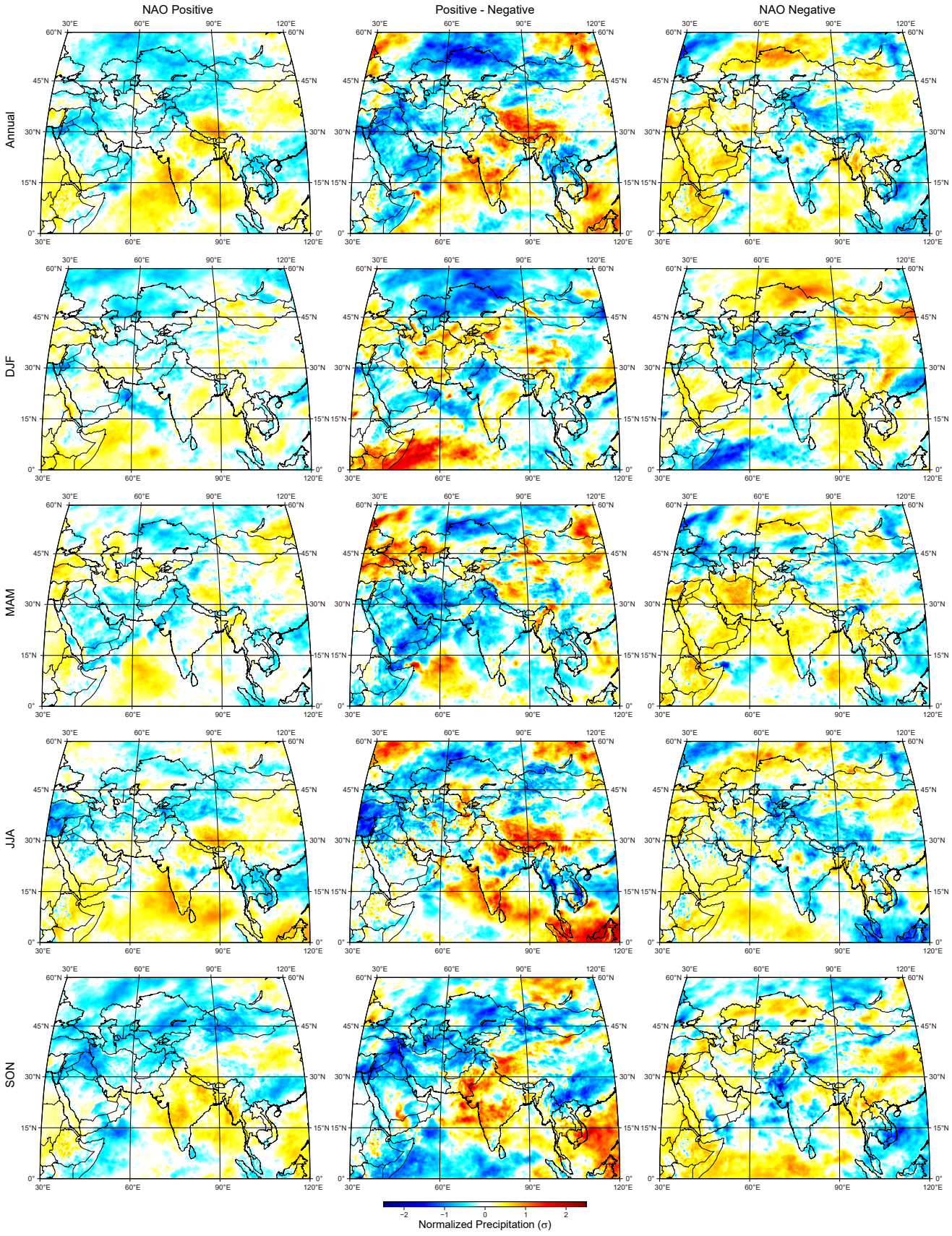

Figure S7. As of Figure S5 but for the ERA5 precipitation (color scale).

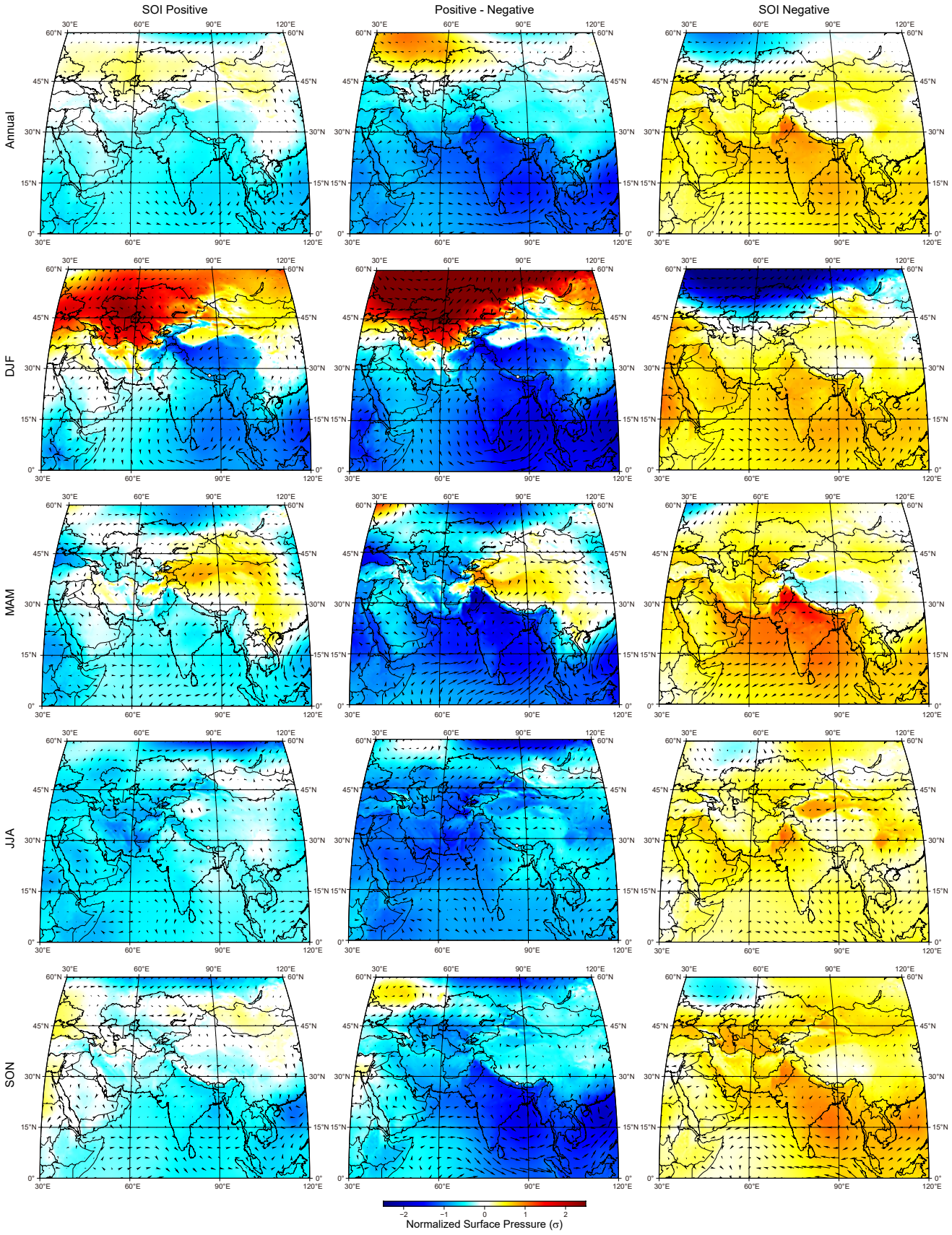

Figure S8. As of Figure S5 but for SOI.

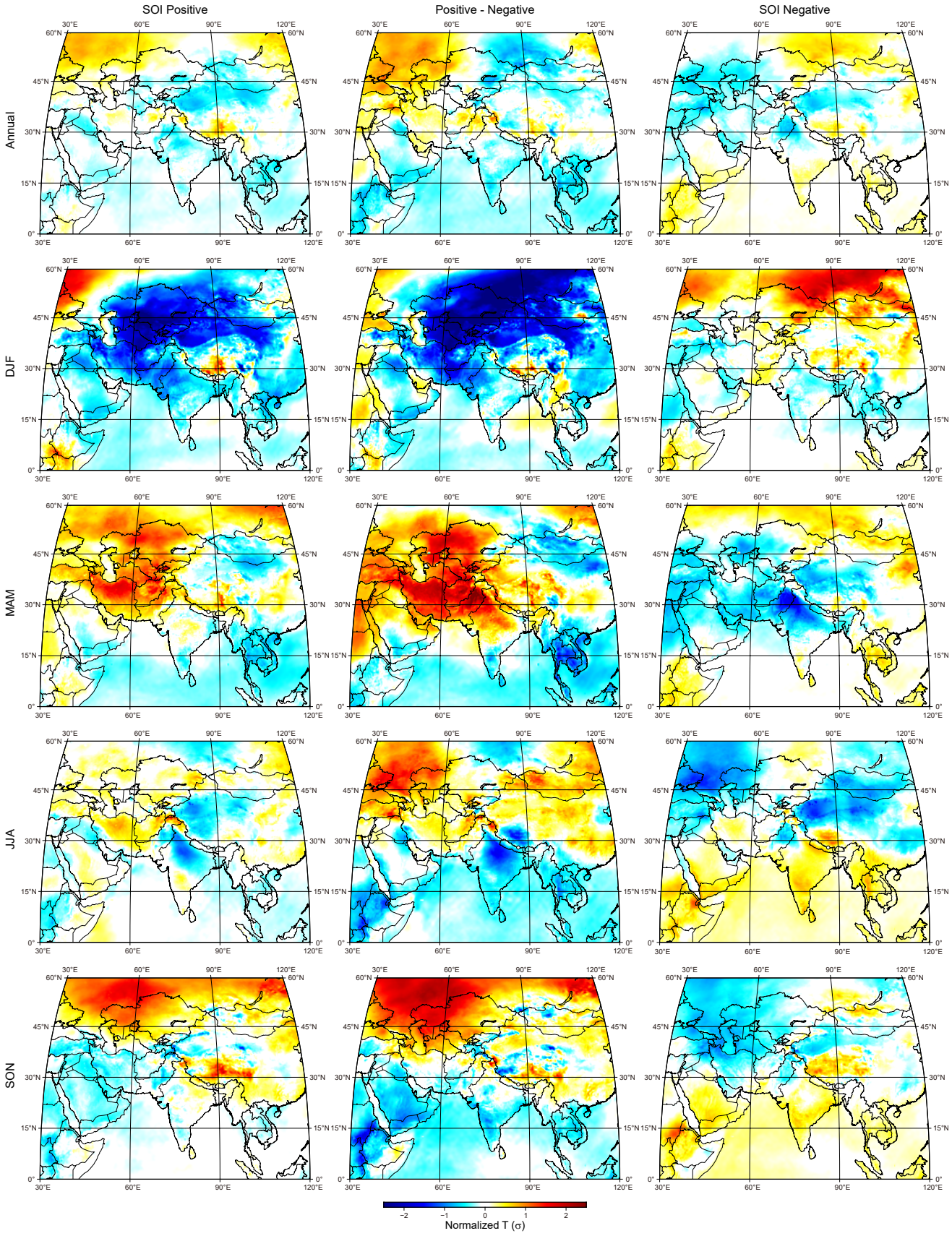

Figure S9. As of Figure S6 but for SOI.

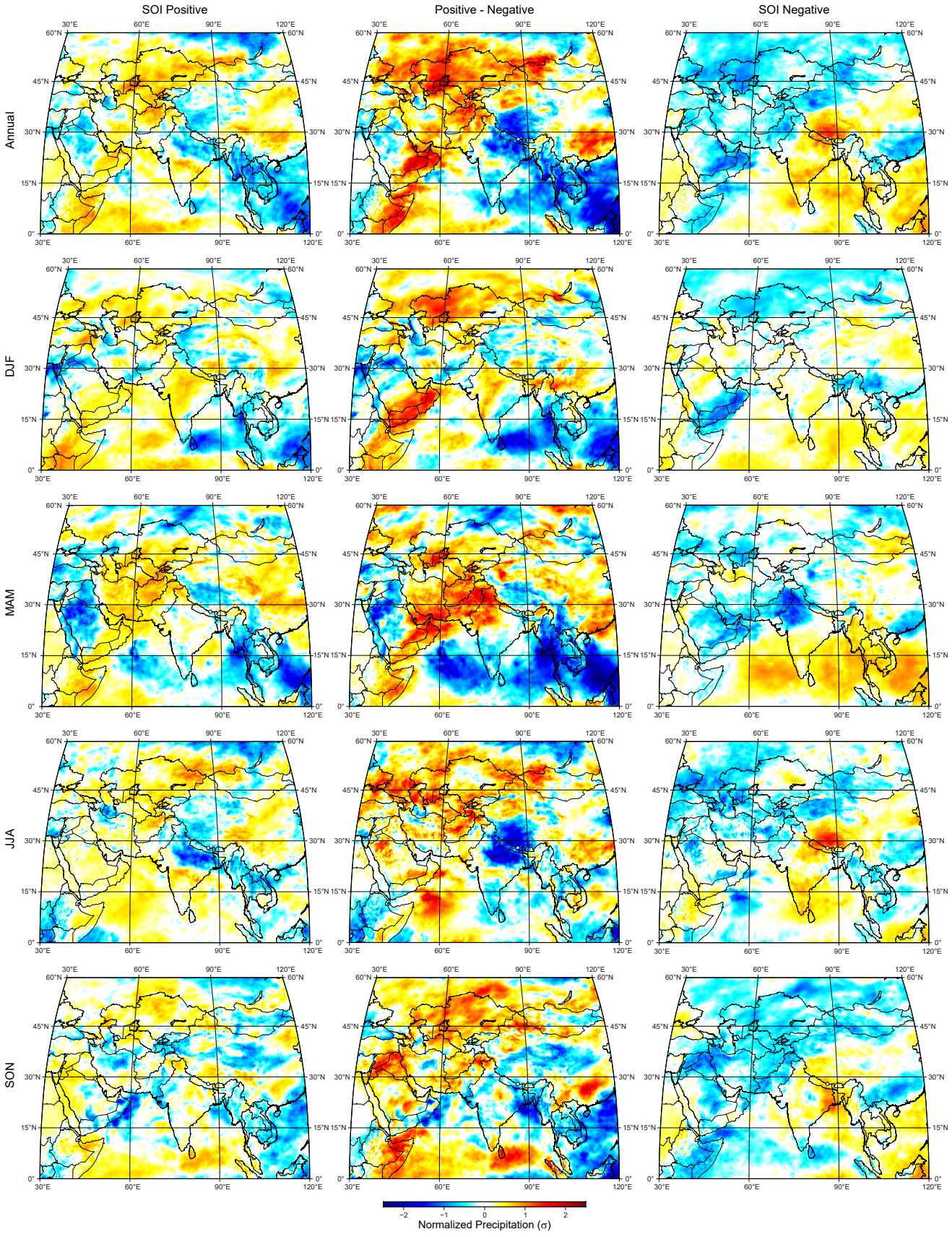

Figure S10. As of Figure S7 but for SOI.